Available online at www.sciencedirect.com
ScienceDirect
Comput. Methods Appl. Mech. Engrg. 361 (2020) 112784
Computer methods in applied mechanics and engineering
www.elsevier.com/locate/cma

Topology optimization method with finite elements based on the k-ε turbulence model

Gil Ho Yoon

School of Mechanical Engineering, Hanyang University, Seoul, Korea

Received 6 December 2018; received in revised form 15 November 2019; accepted 10 December 2019
Available online 30 December 2019

Abstract

A new finite element (FE) based topology optimization (TO) for turbulent flow was developed using the $k-\varepsilon$ turbulent model, which is one of the Reynolds–Averaged Navier–Stokes (RANS) equations. Despite many innovative works on the subject of fluidic TO, it remains important to consider the impact of turbulent flow in TO. To consider the effect of complex turbulent fluid motion, this study considered the $k-\varepsilon$ turbulent finite element model. To conduct a successful TO, the modification of the $k-\varepsilon$ turbulent model to account for the topology evolutions during an optimization process is important. Correspondingly, to account for these effects, we proposed the addition of penalization terms to the original $k-\varepsilon$ turbulent model. To validate the present approach and the effect of turbulent flow on optimized layouts, various two-dimensional designs were optimized by minimizing the turbulent kinetic or the turbulent dissipation energies. Numerical optimization results showed that it is possible to conduct the topology optimization for turbulent flow.

Keywords: Topology optimization; Turbulent flow; RANS model; Finite element method; $k-\varepsilon$ turbulent model

1. Introduction

The purpose of the present study is to develop a new finite element based topology optimization (TO) for turbulent flow using the k–ε turbulent model, which is one of the RANS models [1–6]. Our intent is to contribute to the computational optimization by considering the effect of turbulent flow in two-dimensional design space as an initial research but it can be extended to 3D problem. It is important, challenging, and difficult to simulate and optimize fluidic domains with computational fluid dynamics (CFD) for scientific and engineering applications (see [7–12] and the references therein). Many theoretical and experimental studies have been conducted to understand the complex physics of turbulent flows at various Reynolds numbers. With a small number of optimization variables used to define fixed geometries, the size or the shape optimization problems of turbulent systems considering the complex fluid motions can be accommodated by the development of commercial and open source CFD packages [13,14]. To allow conceptual design changes, the topology or the connectivity of the fluid domain needs to be varied during the optimization process. To date, there have been several important achievements regarding the topology optimization for turbulent flows [2,3,15–18]. To contribute to this research field, this study employs the k–ε turbulent model, which is one of the two-equation turbulent models that statistically averages multiscale eddies, and presents some

E-mail address: gilho.yoon@gmail.com.

https://doi.org/10.1016/j.cma.2019.112784

modifications for fluid TO for turbulent flow and several layout design problems [2,3,8,9,15–20]. In the present study, the finite element-based analysis is employed for the analysis and the proposed optimization, and the involved equations are suggested to be modified in order to consider changes in geometry. The turbulent kinetic energy and the turbulent energy dissipation were considered in the topology optimization problem.

Depending primarily on the magnitude of the Reynolds number, the sequence of flow transitions (defined for a material in nature with zero-shear modulus) includes laminar attached steady flow, laminar separated steady flow, laminar separated periodic flow, laminar separated/turbulent wake periodic flow, and chaotic turbulent separation [1–6,21,22]. The physical characteristics of these flows at different Reynolds numbers are distinct from each other, and a specific theory and computational approach applicable to one flow type may not be pertinent to other types of flows [1,21–23]. Thus, the computational simulation of a fluid with one numerical method should be carried out very carefully based on the in-depth knowledge of the hypothesis, the restriction, and the application scope of the numerical method to obtain physically reasonable computational results. If the computational burden is ignored, it is possible to solve the direct Navier–Stokes (DNS) equation for turbulent fluid, but this requires considerable time and resources, and it seems that its engineering applications are limited (see [1,21–24] and references therein). Owing to the computational burden for the simulation of turbulent flow, many researchers have considered time averaging, and the time variations of velocities and pressure to simplify statistically the energy transportations (energy cascade). Depending on the number of the transportation equations, there exist one-equation turbulent models, two-equation turbulent models, and three-equation turbulent models [1,14,21–24]. The set of transportation equations governing turbulent flow include coupling terms in the form of the destruction and the formulation of expressions of the turbulent kinetic and the dissipation energies.

During the last few years, increasing attention has been paid on topology optimization for turbulent flows. From a topology optimization point-of-view, there exist some innovative published research studies on the topology optimization of turbulent flows [2,3,15–18]. In the pioneering work in [25], a porosity model was developed for topology optimization for a laminar fluid model. In the case of topology optimization that considers incompressible media, some researchers employed mixed finite elements [26–29]. The topology optimization problem has also been solved with a simple kinetic model approximating the Navier–Stokes system [30]. In [31], the level set method for topology optimization was also used for fluid optimization. Additionally, there are some research studies that have been based on the lattice Boltzmann method (LBM) for transient flow [32]. In [2,17,33], the continuous adjoint approach was developed for the S–A turbulent flow model for the first time. Their works should be cited as the first and pioneering works in topology optimization and structural optimization for turbulent flow. In these approaches, the "frozen turbulence" concepts were applied and successfully implemented in OpenFOAM (the simplified modifications of the turbulent eddy viscosity with respect to the design variables). In [18], the topology optimization with turbulent flow was considered to minimize the flow resistance. Additionally, an extensive review of the work that had been performed in this area was presented that included sensitivity analyses with OpenFOAM by overcoming the frozen turbulent assumption. In [34], the adjoint variable approach in OpenFOAM without the frozen assumption was researched for the fluid energy dissipation. In [35], the shape derivative based on topology consideration is presented for the incompressible turbulent flows. In [36], the topology optimization considering aerodynamics was proposed. In [3], the topology optimization for this Spallart–Allamas model was developed. In [37], the topology optimization of unsteady incompressible Navier–Stokes flow was developed and applied the continuous adjoint method. In [38–42], the topology optimization for fluid–structure interactions had also been researched. In the present study, the characteristics (turbulent kinetic energy and fluid energy dissipation) of turbulent flow in topology optimization are considered aiming to contribute to the relevant published research work. To our knowledge, it is challenging and rare to find out optimized topologies considering the turbulent kinetic energy and the turbulent energy dissipation. One of the challenges is to choose between several physical and numerical approaches available. It is important to prove that the basic numerical techniques and the computational grids are reliable and deliver the expected performance in terms of accuracy and convergence. The selection of the appropriate physical model is crucial for the successful simulations and the optimization. This research will investigate some of the effects of the turbulent kinetic energy on the optimized topology with a porosity model with the use of penalization functions.

The present study employs the finite element-based approach for the solution of the k–ε turbulent model, proposes some modifications of the original the k–ε turbulent model to allow spatially varying topologies, and shows the effects of turbulent flows in topology optimization. For a successful TO method, some necessary conditions should be derived regarding fluid velocities, pressure, and some other parameters pertaining to the solid and fluid domains,

and these conditions should be imposed to these solid and fluid domains. For the solid domains, fluid velocities and associated energies should be set to zero. To satisfy these conditions, we added some modifications to the original k–ε turbulent model and interpolated the involved material properties with respect to the spatially varying design variables. Through these changes, optimized topologies can be designed for turbulent flows.

This study is organized as follows: Section 2.1 describes the basic equations for turbulent flow and the k–ε turbulent model. Section 2.2 describes our development of the present k–ε turbulent model for topology optimization. In Section 3, we present several optimization examples to show the advantages and disadvantages of the present procedure in TO. In Section 4, we present our conclusions and suggest directions for future research topics.

2. FE-based turbulent flow simulation and formulation of the topology optimization

2.1. FE-based simulation of turbulent flow

Several numerical approaches are viable in the simulation of turbulent flow, including direct numerical simulations (DNS) of turbulent flow, LES (large eddy simulations), and the Reynolds–averaged Navier–Stokes equations (RANS) proposed by Osborne Reynolds [8,13,22,23], that assumes the statistical time-averaged equations of motion for fluid flow. The DNS are based on the direct use of the Navier–Stokes equation with a small-scale mesh that requires tremendous computational resources [7,8,10–14,19–24,43,44]. The computational cost increases as Re^3 with the Kolmogorov length and time scales and it is restricted to flow with low or moderate Reynolds numbers. In LES, a filtered velocity field for the large-scale turbulent motion is considered and solved. The RANS theory accepts the statistical decompositions of instantaneous velocity and pressure into their time-averaged and fluctuating quantities. Furthermore, it assumes the existence of statistically isotropic turbulence. In a turbulent flow, it is discovered that an energy cascade occurs. In other words, the unstable large eddies break up and transfer their energies to smaller eddies. Thus, these smaller eddies also break up and transfer their energies to even smaller eddies. In the DNS simulation, the cascade energy transformation can be directly simulated while the RANS solves the dissipation of the energy by the molecular viscosity of fluid.

In the RANS simulation, the Boussinesq hypothesis for the additional unknown fluctuating term is adopted, i.e., the simple relationship between Reynolds stresses and velocity gradients that uses the scalar and isotropic eddy viscosity, μ_{T}. The Reynolds stress tensor S_{ij} is linearly related to the time-averaged rate of strain using the scalar turbulent viscosity.

$$\text{Boussinesq hypothesis: } R_{ij} = -\rho\overline{u_i' u_j'} = 2\mu_{\mathrm{T}} S_{ij} \quad S_{ij} = \frac{1}{2}\left(\frac{\partial u_i}{\partial x_j} + \frac{\partial u_j}{\partial x_i}\right) \tag{1}$$

The resulting NS equation after the above procedures are implemented with the use of the average terms can be stated as follows,

$$\rho u_i \frac{\partial u_i}{\partial x_j} = -\frac{\partial p}{\partial x_i} + \frac{\partial}{\partial x_j}\left((\mu + \mu_{\mathrm{T}})\frac{\partial u_i}{\partial x_j}\right), \frac{\partial u_i}{\partial x_i} = 0 \tag{2}$$

The time-averaged velocity and pressure terms are $u_i(x, y, z)$ and $p(x, y, z)$, respectively. The fluid density is denoted by ρ. The tensor form is given as follows,

$$\overbrace{\rho(\mathbf{u}\cdot\nabla)\mathbf{u}}^{\text{Convective acceleration}} = \underbrace{\nabla\cdot\left[-p\mathbf{I} + (\mu+\mu_{\mathrm{T}})(\nabla\mathbf{u} + \nabla\mathbf{u}^{\mathrm{T}})\right]}_{\text{Divergence of stress}} \tag{3}$$

$$\nabla\cdot\mathbf{u} = 0$$

To obtain and capture interesting quantities with a trackable engineering model, it is an issue how to define the constant and isotropic eddy viscosity which reflects *turbulent energy dissipations* in (3). Many approximation theories have been developed depending on the physical interpretation of the eddy viscosity models with the time-averaged velocity gradients for particular scientific and engineering applications. Depending on the simulation conditions and the limitations of the models, an engineer should choose a proper turbulent model after understanding the limitation of the model. As a simple measure, they can be classified in terms of the number of the transport equations solved in addition to the NS equations, i.e., the zero-equation or the algebraic model, one-equation models, two-equation models, three-equation models, and four-equation models [12,14,21].

In the case of the zero-equation model, the Prandtl's mixing length, the Smagorinsky model for the subgrid scale eddy, the Cebeci–Smith model, and the Baldwin–Lomax model, have all been developed. In the case of the one-equation model, Woflstein, Baldwin–Barth, Spalart–Allmaras (S–A), and k-models, have been developed. Correspondingly, in the case of the two-equation models, the standard k–ε, k–ω, k–τ, and k–L models have been developed. Furthermore, a three-equation model, namely, the k–ε–A model, and a four-equation model, namely, the v^2–f model, have also been developed. More details on these studies can be retrieved from ([2,11,14,16,17,21]). In the present study, we employed the k–ε turbulent model for fluid topology optimization.

2.2. FE based k–ε turbulent model

One of the distinct features of the two-equation turbulent models is that two separate transport equations are formulated and solved. The standard k–ε turbulent model can be formulated by considering the turbulent kinetic energy (k) and the turbulent energy dissipation (ε) as the unknown variables, in addition to the time-averaged fluid velocities. By computing these energies, the length scale ($\sim k^{3/2}/\varepsilon$), and the eddy viscosity ($\sim k^2/\varepsilon$), can be computed. With some constants and the coupling terms, the turbulent kinetic energy and the turbulent dissipating energy of the stationary k–ε model are formulated as follows,

$$\frac{\partial(\rho k u_i)}{\partial x_i} = \frac{\partial}{\partial x_j}\left[\left(\mu + \frac{\mu_t}{\rho_k}\right)\frac{\partial k}{\partial x_j}\right] + P_k - \rho\varepsilon,\ \rho_k = 1 \tag{4}$$

$$\frac{\partial(\rho \varepsilon u_i)}{\partial x_i} = \frac{\partial}{\partial x_j}\left[\left(\mu + \frac{\mu_t}{\rho_\varepsilon}\right)\frac{\partial \varepsilon}{\partial x_j}\right] + C_{1\varepsilon}\frac{\varepsilon}{k}P_k - C_{2\varepsilon}\rho\frac{\varepsilon^2}{k},\ C_{1\varepsilon} = 1.44,\ C_{2\varepsilon} = 1.92,\ \rho_\varepsilon = 1.3 \tag{5}$$

$$\mu_t = \rho C_\mu \frac{k^2}{\varepsilon},\ C_\mu = 0.09,\ P_k = \mu_t 2 S_{ij} S_{ij},\ S_{ij} = \frac{1}{2}\left(\frac{\partial u_j}{\partial x_i} + \frac{\partial u_i}{\partial x_j}\right) \tag{6}$$

where the turbulent kinetic energy and the turbulent energy dissipation tensors can be defined as follows

$$\begin{aligned} &\rho(\mathbf{u}\cdot\nabla)\mathbf{u} = \nabla\cdot\left[-p\mathbf{I} + (\mu + \mu_{\mathrm{T}})(\nabla\mathbf{u} + \nabla\mathbf{u}^{\mathrm{T}})\right] \\ &\nabla\cdot\mathbf{u} = 0 \end{aligned} \tag{7}$$

$$\rho(\mathbf{u}\cdot\nabla)k = \nabla\cdot\left[\left(\mu + \frac{\mu_{\mathrm{T}}}{\rho_k}\right)\nabla k\right] + P_k - \rho\varepsilon \tag{8}$$

$$\rho(\mathbf{u}\cdot\nabla)\varepsilon = \nabla\cdot\left[\left(\mu + \frac{\mu_t}{\rho_\varepsilon}\right)\nabla\varepsilon\right] + C_{1\varepsilon}\frac{\varepsilon}{k}P_k - C_{2\varepsilon}\rho\frac{\varepsilon^2}{k} \tag{9}$$

where $\mathbf{u}$ is the fluid velocity vector in ms^{-1} and the divergence operator is represented using the symbol ∇. To solve the above k–ε turbulent model, a finite element procedure can be applied. The second-order shape functions are employed for the velocities and for the kinetic and the dissipation energy, while the linear shape function is employed for the pressure as shown in Fig. 1. To identify a steady-state solution with an nonoptimal condition number, the velocity, cell-size, and a time step, should be considered in configuring the Courant–Friedrichs–Lewy condition (CFL) for the nonlinear solver. The CFL number determining the length over which turbulent flow travels within a time step should be equal to a fraction of the mesh element size, and is important in identifying a steady state solution. For a more accurate enforcement of the CFL condition we should ensure a smaller error for the approximation of the time derivative compared to the approximation of the spatial derivative.

2.3. Modifications of the k–ε turbulent model for topology optimization

One of the representative features of topology optimization is that we allow topology changes inside the design domains [15,40,45]. To make it possible, it is necessary to add some modifications to the original k–ε governing equations with respect to the spatially varying design variables. The most popular interpolation function may be the SIMP (Solid Isotropic Material with Penalization) function. With it, for example, Young's modulus, thermal conductivity, or electric conductivity can be interpolated for structural, heat transfer, or electrostatic problems, respectively. For laminar fluid problems, an additional force term, sometimes referred to as the Darcy force, the damping force, or the Lagrange force, is added to the direct NS equations.

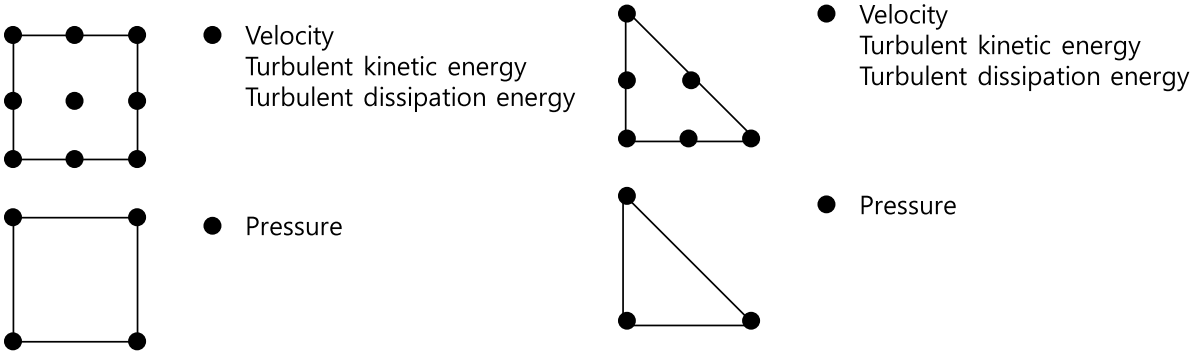

Fig. 1. Finite element discretization.

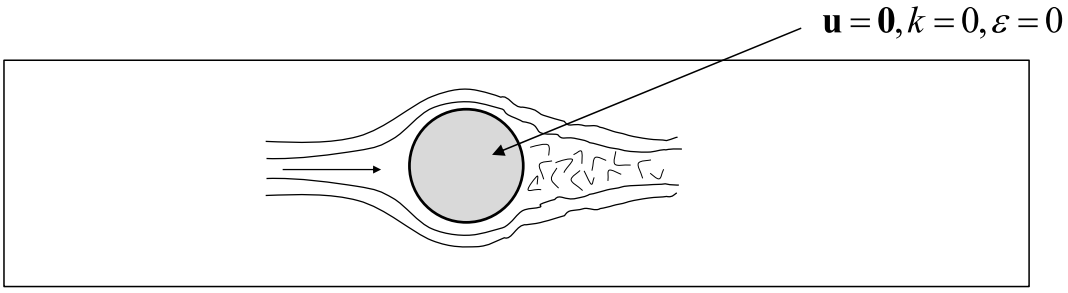

Fig. 2. Material interpolation of solid domain.

Regardless of any interpretation for these forces added to the NS equations, they are supplementary to enforce the velocities of solid domains smaller values near zero for the zero-velocity or the no-slip condition [25,26,37,41,46–53]. In [3], the SA model is modified for topology optimization and in [18], the k–ε turbulent model is modified for topology optimization. The present study adopts the similar ideas in [18] to modify the turbulent equations for topology optimization and we consider the topology optimization problem controlling the energies. The original k–ε turbulent equations also should be modified to allow free material distribution. To achieve this, the special conditions of the k–ε turbulent models, i.e., the fluid velocities become zeros and the turbulent kinetic energy and the turbulent energy dissipation become k_0 and ε_0, for a solid domain are imposed as shown in Fig. 2 as follows:

$$\rho(\mathbf{u}\cdot\nabla)\mathbf{u} = \nabla\cdot\left[-p\mathbf{I}+(\mu+\mu_{\mathrm{T}})(\nabla\mathbf{u}+\nabla\mathbf{u}^{\mathrm{T}})\right] + \underbrace{\alpha(\gamma)\mathbf{u}}_{\text{Added penalty term}}$$
$$\nabla\cdot(\rho\mathbf{u}) = 0 \tag{10}$$

$$\rho(\mathbf{u}\cdot\nabla)k = \nabla\cdot\left[\left(\mu+\frac{\mu_{\mathrm{T}}}{\rho_k}\right)\nabla k\right] + P_k - \rho\varepsilon\underbrace{-\alpha^k(\gamma)(k-k_0)}_{\text{Added penalty term}} \tag{11}$$

$$\rho(\mathbf{u}\cdot\nabla)\varepsilon = \nabla\cdot\left[\left(\mu+\frac{\mu_t}{\rho_\varepsilon}\right)\nabla\varepsilon\right] + C_{1\varepsilon}\frac{\varepsilon}{k}P_k - C_{2\varepsilon}\rho\frac{\varepsilon^2}{k}\underbrace{-\alpha^\varepsilon(\gamma)(\varepsilon-\varepsilon_0)}_{\text{Added penalty term}} \tag{12}$$

$$\begin{aligned}&0(\text{Solid}) \le \gamma \le 1(\text{Fluid}),\ \alpha = (\alpha_{\max}-\alpha_{\min})\tfrac{q_u(1-\gamma)}{(\gamma+q_u)} + \alpha_{\min}\\ &\alpha^k = (\alpha^k_{\max}-\alpha^k_{\min})\tfrac{q_k(1-\gamma)}{(\gamma+q_k)} + \alpha^k_{\min},\ \alpha^\varepsilon = (\alpha^\varepsilon_{\max}-\alpha^\varepsilon_{\min})\tfrac{q_\varepsilon(1-\gamma)}{(\gamma+q_\varepsilon)} + \alpha^\varepsilon_{\min}\end{aligned} \tag{13}$$

The spatially varying design variable is denoted by γ and it is used to interpolate the penalization parameters in (13) [25,26,37,41,46–52]. In Eq. (10), i.e., the momentum equation, the Darcy force terms, $\alpha\mathbf{u}$, are added with the maximum factor, $\alpha_{\max}$, and the minimum factor, $\alpha_{\min}$, while similar forces are added in the transportation equations in (11) and (12). In the transportation equations (11) and (12), the penalization terms are added to impose some

values for the kinetic and the dissipation energy. These penalization factors often cause the instability in analysis and the penalizations should be carefully modeled. In the present study, several coefficients are tested to get the optimized layouts. In real fluid systems, the energies and the velocities vary from one point to another both in magnitude and direction (see [54] and references therein). Although the above values vary in nature for turbulent flows, the numerical treatment of this issue becomes a significant challenge. It should be mentioned that this research assumes constant values for the velocities and the energies inside the solid domain and that the boundary conditions are enforced weakly. Also it should be mentioned that Eq. (13) is to interpolate the solid material resistance force with respect to the design variable. The solid conditions are imposed with zeros for the design variables and the fluid conditions are imposed with ones for the design variables. It is not clear about the physical conditions of the intermediate design variables and it is important to obtain solid and fluid designs after the optimization. Another point is imposing the wall function along rigid boundaries. The wall provides rise to a boundary layer where the velocity changes from the no-slip boundary condition at the wall to its free stream value. The near-wall region can be divided into viscous sub-layer ($0 < y^+ < 5$), buffer layer ($0 < y^+ < 30$), and inertial sub-layer ($30 < y^+ < 200$). Inside the viscous sub-layer, the turbulence effects can be ignored while the viscous effects become relatively small in the inertial sub-layer. The turbulent and viscous effects become significant in the buffer layer. The velocity variation is usually largest in the near-wall region with the strongest gradients. One approach is to use a very fine mesh close to the wall to resolve the flow and capture the flow gradients. From an engineering point of view, this becomes expensive and a numerical approach bridging the near-wall region is introduced. In the present approach, the wall condition is not implemented along solid domains due to the difficulties in the implementation and the sensitivity analysis.

Solution procedure and sensitivity analysis

The sensitivity values are computed by the adjoint method, and the optimization problem considers that the feature of turbulent flow is solved by a gradient-based algorithm. To obtain the sensitivity of a specific quantity with respect to the variations in the design variable in the analytical sensitivity analysis, the adjoint variable method is employed [5,15,16]. The state variables, fluid velocities, pressure, turbulent kinetic energy, and turbulent energy dissipation, are denoted by $\mathbf{S}$. With an objective function, ϕ, the sensitivity value can be defined using the Lagrange multiplier, $\boldsymbol{\lambda}$.

$$L = \phi + \boldsymbol{\lambda}^{\mathrm{T}}\mathbf{R} \text{ and } \mathbf{R}(\mathbf{S}) = \mathbf{0} \tag{14}$$

where the residual vector of the governing equation is denoted by $\mathbf{R}$. To solve the equilibrium equation, the pseudo-time stepping approach can be used [55].

$$\mathbf{R}(\mathbf{S}) = \mathbf{0} \Rightarrow \frac{d\mathbf{S}}{dt} = \mathbf{R}(\mathbf{S}), \mathbf{S}(0) = \mathbf{S}_0, \lim_{t\to\infty} \mathbf{S}(t) = \text{Steady state solution} \tag{15}$$

The derivatives of the Lagrange L with respect to the design variable and subject to the constraint $\mathbf{R}(\mathbf{S}) = \mathbf{0}$, are formulated as follows,

$$\frac{\partial \phi}{\partial \mathbf{S}} + \boldsymbol{\lambda}^{\mathrm{T}}\frac{\partial \mathbf{R}}{\partial \mathbf{S}} = \mathbf{0} \tag{16}$$

$$\frac{dL}{d\boldsymbol{\gamma}} = \frac{\partial \phi}{\partial \boldsymbol{\gamma}} + \boldsymbol{\lambda}^{\mathrm{T}}\left(\frac{\partial \mathbf{R}}{\partial \boldsymbol{\gamma}}\right) + \left(\frac{\partial \phi}{\partial \mathbf{S}} + \boldsymbol{\lambda}^{\mathrm{T}}\frac{\partial \mathbf{R}}{\partial \mathbf{S}}\right)\frac{d\mathbf{S}}{d\boldsymbol{\gamma}} \tag{17}$$

It is clear that the term, $\frac{\partial \mathbf{R}}{\partial \mathbf{S}}$, becomes the tangent stiffness matrix of the nonlinear governing equations. The appendix illustrates an example of the sensitivity analysis. The optimization procedure can then be developed based on the script implementation using FE in COMSOL [56]. The state variables, $\mathbf{S}$, are the vectors containing the fluid velocity, the pressure, the turbulent kinetic energy and the turbulent dissipation energy. Each equation of the adjoint system for the given objective function can be defined with respect to these state variables and the automatic differentiation of the software can be incorporated with the implementation of the adjoint system; the adjoint equations for the turbulent kinetic energy and the turbulent dissipation energy should be additionally included to the adjoint equations of the fluid velocity and the pressure. We should mention that it may be possible to include the frozen turbulence technique consists of not using the sensitivity of the eddy viscosity for the sensitivity of the RANS equation for future research.

The simulation of the turbulent flow used to identify a steady state solution in the finite element procedure is very challenging, especially for very low CFL, a nonoptimal condition number, a transient solution, and in the case where

a steady-state solution does not exist. Therefore, we can try the optimization with a low-Reynolds number using low-penalization values as indicated in (13). We can then continue the optimization process with a high-Reynolds number. However, the referred approaches were not applied to the examples.

To verify the numerical approach described above, we solved the channel problem with the expansion chamber in Fig. 3. To compare the solutions, we set $\boldsymbol{\gamma} = 0$ (solid) at the expansion chambers and the obtained velocities, pressure, and energies, are compared in Fig. 3. Some distributions of the turbulent kinetic energy, the turbulent energy dissipation and the turbulent viscosity at the several locations are compared in Fig. 4. As illustrated, the developed approach can be employed for topology optimization for turbulent flows.

3. Topology optimization examples

To show the validity of the present TO formulation, this section presents several topology optimization examples considering the effects of turbulent flow (the fluid is air in the examples). The optimization formulations with the turbulent kinetic and the dissipation energies are considered as an aeroacoustics phenomenon, vibrations owing to turbulent flow and some other related engineering problems are highly dependent on the characteristics of the energies. To our best knowledge, it is rare to consider these energies in topology optimization. Therefore, the design with the control of these energies is important from an engineering point-of-view. For example, in aeroacoustics engineering, the average acoustic intensity, $\mathrm{I} = \frac{\langle p^2 \rangle}{\rho c}$, is sometimes assumed to be a function to the turbulent energy dissipation and the Mach number $M = u/c$, i.e., $r^2 I/V \sim \rho \varepsilon M^5$, where r is the distance, and V is the volume of turbulent flow [57]. To the best of our knowledge, it is rare to endorse this assumption in topology optimization considering the energies. The upper limits of the penalization in (13) are set to 100, and the penalization factors, q_u, q_k, and q_ε, are set to a value between 0.01 and 0.1.

Example 1: A simple channel design (air flow with Reynolds number = 4.4014 x 10^4)

For the first numerical example, we consider the simple channel or the channel design in Fig. 5. The following optimization formulation of (18) minimizing the integration of the kinetic turbulence energy inside the objective domain subject to the mass constraint is solved by the method of moving asymptotes [58].

$$\begin{aligned} &\underset{\boldsymbol{\gamma}}{\text{Minimize}}\ \phi = \int_{\Omega_{obj}} k d\Omega \\ &\text{Subject to } V_{Solid} = \int_{\Omega} (1-\gamma) d\Omega \le V^0 \qquad (\underset{\text{Solid}}{0} \le \gamma_i \le \underset{\text{Fluid}}{1}) \end{aligned} \tag{18}$$

The volume of the solid and the upper limit of the mass usage are denoted by V_{Solid} and V^0, respectively. The ith design variables varying from 0 (solid) to 1 (fluid) are denoted by γ, respectively. The integration turbulent kinetic energy inside the objective domain denoted by Ω_{obj} is set as an objective function. To the best of our knowledge, the topology optimization controlling the turbulent kinetic energy has been rarely applied previously [25,47,48]. The consideration of the turbulent kinetic energy does have some importance in some engineering applications regarding noise or drag reductions. Characteristically, there have been some research studies that aimed at the prediction of an approximate level of flow noise using CFD, and there have been some empirical formulations with the kinetic turbulent energy [59]. Therefore, the optimized layouts of the above optimization formulation can have some implications in engineering design processes.

Fig. 5 shows the design and the analysis domains and the simulation conditions. It is assumed that air flow ($\rho = 1.25\,\mathrm{Kg/m^3}$, $\mu = 1.42 \times 10^{-5}\,\mathrm{m^2/s}$) moves from the left side to the right open side with a velocity of 0.5 m/s. The inlet kinetic and the dissipation energies are arbitrarily set at $k_{in} = 0.19\,\mathrm{m^2/s^2}$ and $\varepsilon_{in} = 1.98 \times 10^{-3}\,\mathrm{m^2/s^3}$, respectively, these are used in order to model complicated and random turbulent flows containing eddying motions of all sizes originating from a faucet or an orifice, whereby a large part of the mechanical energy in the flow goes into the formation of these eddies. Based on the material properties and the characteristic length (see Fig. 5), the estimated Reynolds number is approximately equal to 4.4014×10^3 that is indicative of turbulent flow. To identify a steady-state flow with this Reynolds number based on the finite element procedure, the standard Newton–Raphson iteration suffers from convergence issues, and the pseudo-time stepping approach for the stabilization and acceleration should be thus employed using an initial, low-value guess estimate (initial CFL number ≤ 3, PID regulator proportional ≤ 0.65, PID regulator derivative ≤ 0.05, PID regulator integrative ≤ 0.05). The pseudo-time stepping approach is one of the solution approaches modified from the Newton–Raphson iteration to enhance the

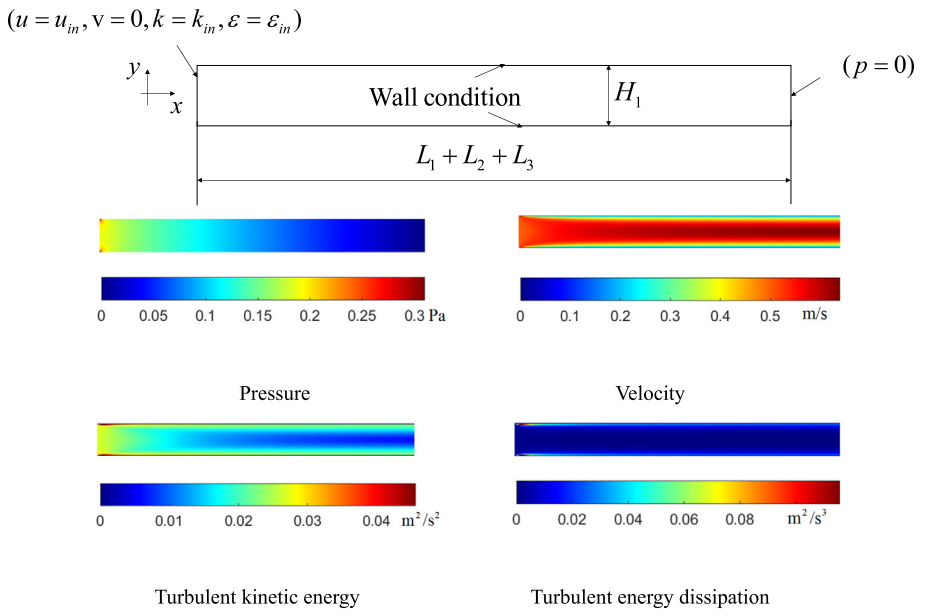

(a) continued

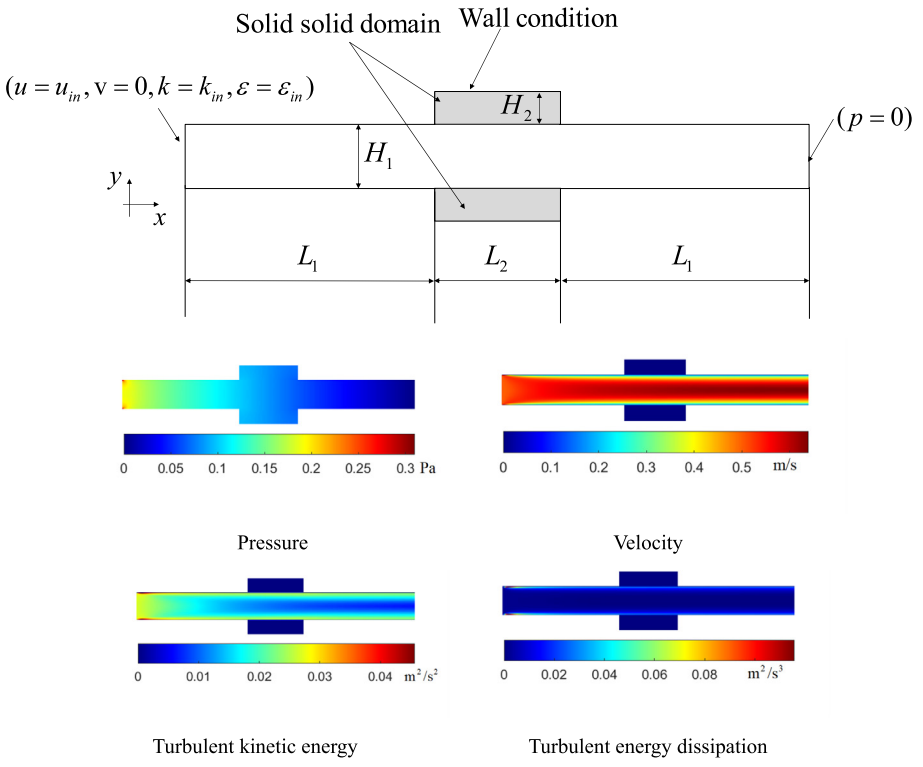

(b)

Fig. 3. A verification of the modeling of (10)–(13) with a channel analysis example. (a) Analysis without the modifications and (b) analysis with the modifications. ($\rho = 1.25\,\mathrm{kg/m^3}$, $\mu = 1.42 \times 10^{-5}\mathrm{Pa \cdot s}$, $L_{RE} = 1\,\mathrm{m}$, $u_{in} = 0.5\,\mathrm{m/s}$, Reynolds number: 4.4014×10^4 ($\mathrm{Re} = \frac{\rho u L_{\mathrm{RE}}}{\mu} = \frac{1.25 \times 0.5 \times 1}{1.42 \times 10^{-5}}$), $k_0 = 0$, $\varepsilon_0 = 0$, mesh size $= 0.0625$ m by 0.0625 m, $L_1 = 4\,\mathrm{m}$, $L_2 = 2\,\mathrm{m}$, $H_1 = 1\,\mathrm{m}$, $H_2 = 0.6240\,\mathrm{m}$ $k_{in} = 0.19\,\mathrm{m^2/s^2}$ and $\varepsilon_{in} = 1.98 \times 10^{-3}\,\mathrm{m^2/s^3}$, $\alpha_{\max} = \alpha^k_{\max} = \alpha^\varepsilon_{\max} = 100$, $\alpha_{\min} = \alpha^k_{\min} = \alpha^\varepsilon_{\min} = 0$).

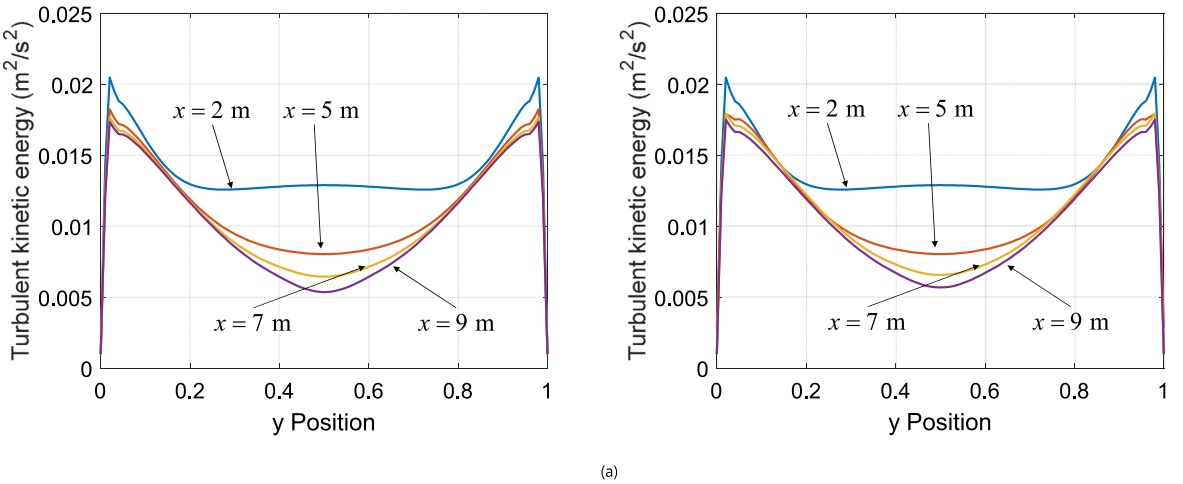

(a)

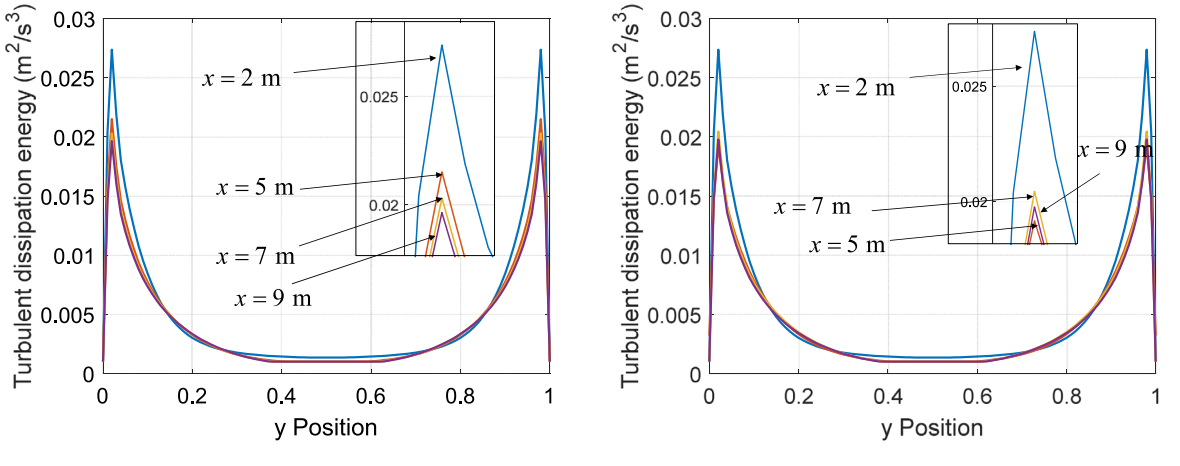

(b)

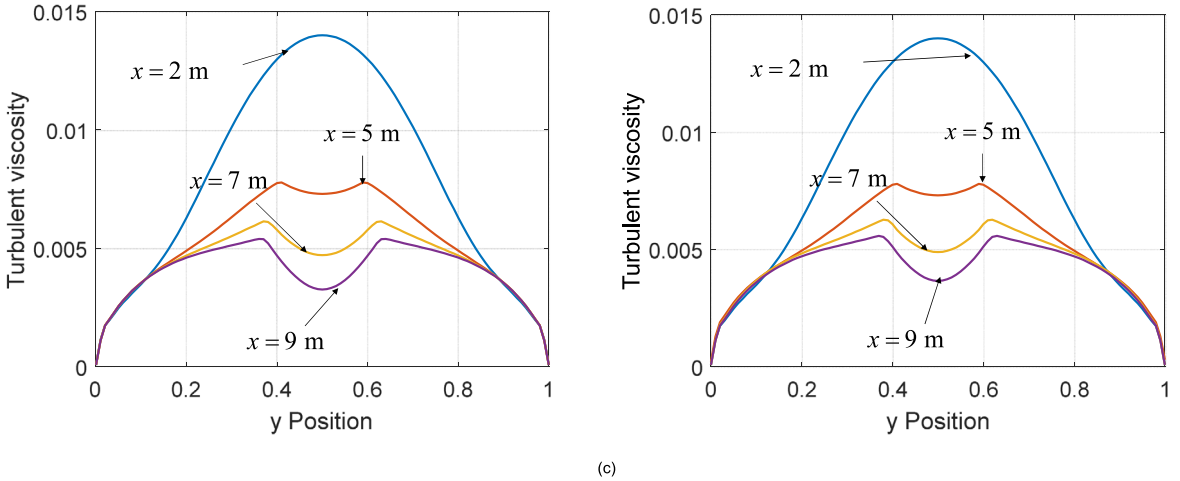

(c)

Fig. 4. The comparisons of the turbulent kinetic energy, the turbulent energy dissipation and the turbulent viscosity (Left: Fig. 3(a), Right: Fig. 3(b)).

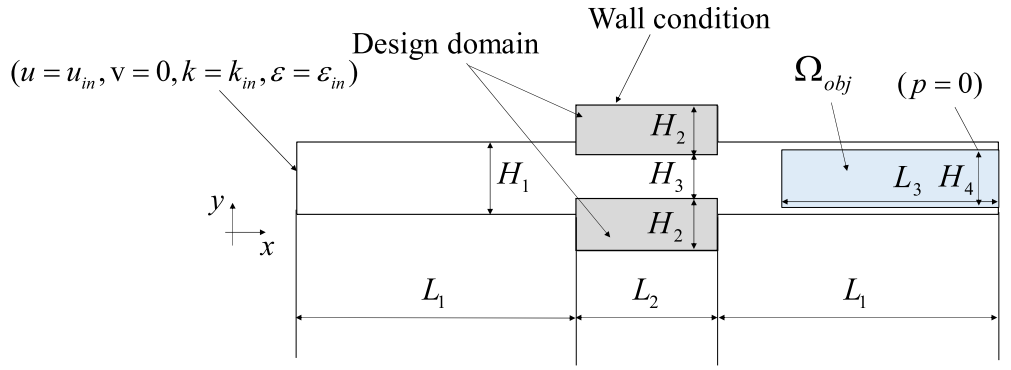

Fig. 5. Channel design problem definition for topology optimization minimizing the turbulent kinetic energy or the energy dissipation of the objective domain. (Air: $\rho = 1.25\,\mathrm{kg/m^3}$, kinematic viscosity $= 1.42 \times 10^{-5}\mathrm{Pa \cdot s}$, $L_{RE} = 1\,\mathrm{m}$, $u_{in} = 0.5\,\mathrm{m/s}$, Reynolds number: 4.4014×10^4(Re $= \frac{\rho u L_{\mathrm{RE}}}{\mu} = \frac{1.25 \times 0.5 \times 1}{1.42 \times 10^{-5}}$), $k_0 = 0$, $\varepsilon_0 = 0$, mesh size $= 0.0625$ m by 0.0625 m, $L_1 = 4\,\mathrm{m}$, $L_2 = 2\,\mathrm{m}$, $H_1 = 1\,\mathrm{m}$, $H_2 = 0.6240\,\mathrm{m}$, $H_3 = 0.75\,\mathrm{m}$, $H_4 = 0.80\,\mathrm{m}$, $V^0 = 50\%$, $k_{in} = 0.19\ \mathrm{m^2/s^2}$ and $\varepsilon_{in} = 1.98 \times 10^{-3}\ \mathrm{m^2/s^3}$).

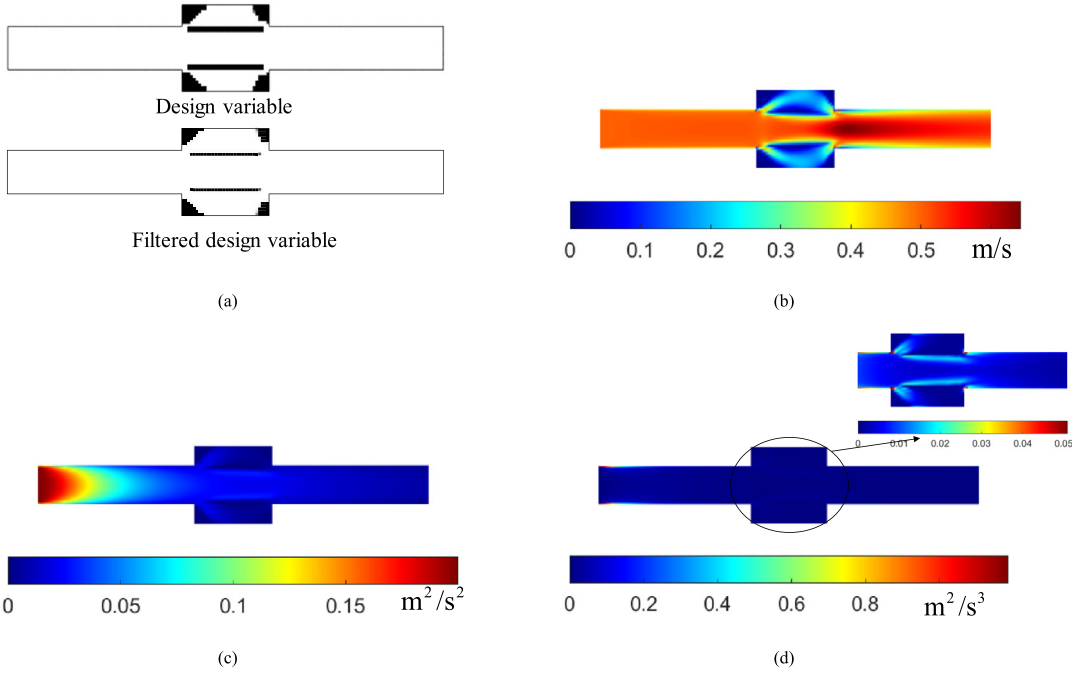

Fig. 6. An optimized design for the channel design. (a) The optimized layout, (b) the fluid velocity, (c) the turbulent kinetic energy and (d) the turbulent energy dissipation.

convergence [55]. The adjoint sensitivity analysis requires the tangent stiffness matrix of the solution by the pseudo-time stepping approach. Furthermore, the maximum values of the parameters in (13) influence the convergence of the solution. From our numerical setting, some higher values of the maximum values often cause unconvergences and we require the isotropic diffusions for solutions. It was assumed that there were two rectangular boxes in the middle of the channel in accordance to the design domain, which were discretized using $0.0625\ \mathrm{m} \times 0.0625\ \mathrm{m}$ rectangular meshes. We assumed that the velocity and the kinetic and dissipation energies became zero at the boundary surface of the solid domains. The objective was then to identify optimized topologies at the design domains for the optimization formulation in (18). Figs. 6 and 7 show an optimized layout of this problem and some intermediate designs. The design filled with fluid ($\gamma = 1$) denotes the initial design with the dilation morphological filter with $r_{\min} = 1.5\times$ element size. The sensitivity filter is not applied. At the optimization step around the 10th step, the shape of a bird

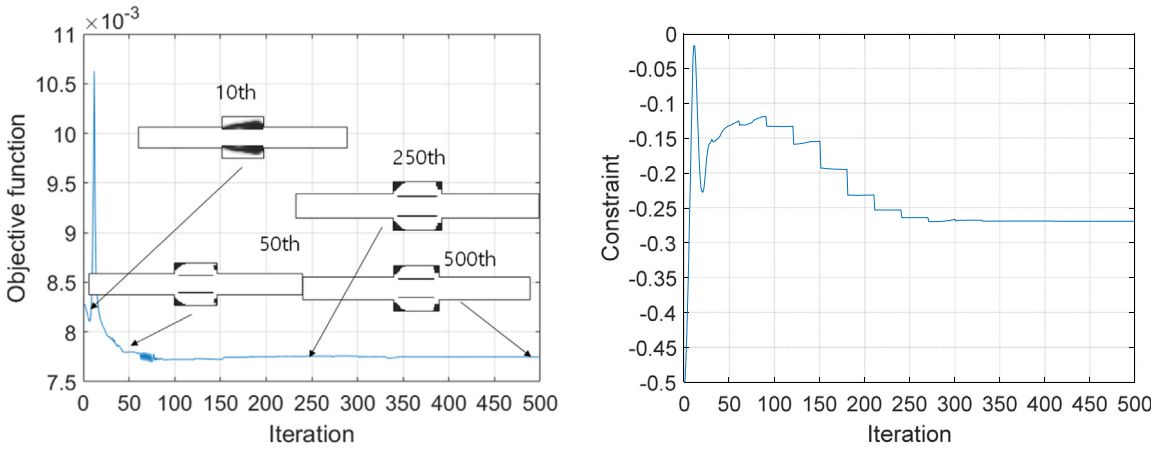

(a) (b)

Fig. 7. The convergence histories of the objective and the constraint for the channel design example in Fig. 5.

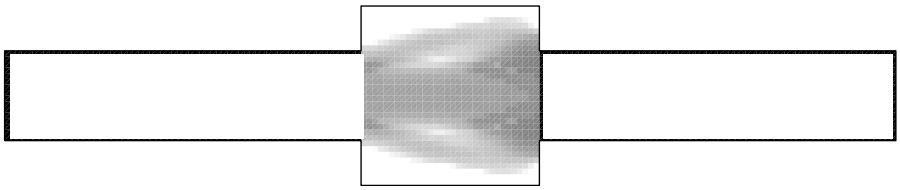

Fig. 8. Optimized membrane layout with the enlarged design domain (optimization procedure termination was due to the numerical errors in the analysis and optimization).

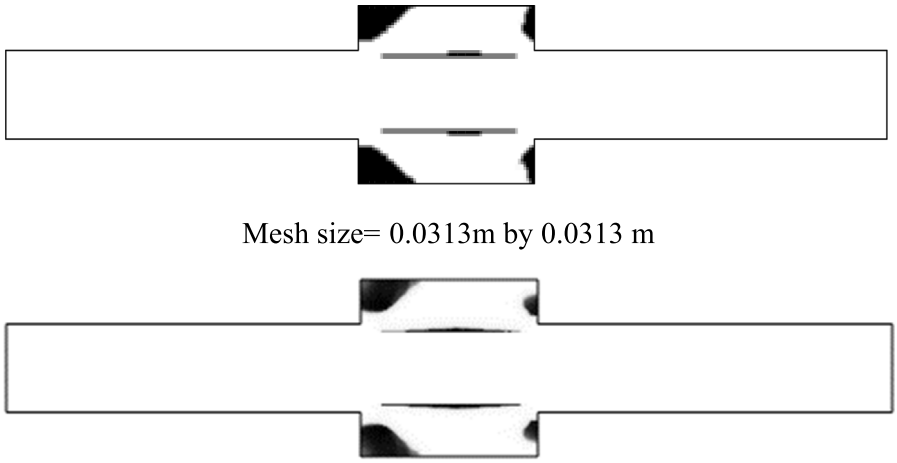

Fig. 9. Optimized design with refined mesh (0.0313 m by 0.0313 m and mesh size = 0.015625 m by 0.015625 m in this RANS model where the Kolmogorov length scale $(\eta = \left(v^3/\varepsilon\right)^{1/4} \sim 0.001$ m for DNS).

tomium appears along the channel, but its shape changes to the two straight lines with the detour channels. The mass constraint is not active and it converges to a value that is approximately equal to -0.26. This implies that the fluid design ($\gamma = 1$) is not an optimized layout for the formulation of (18), and the optimizer identifies the optimal

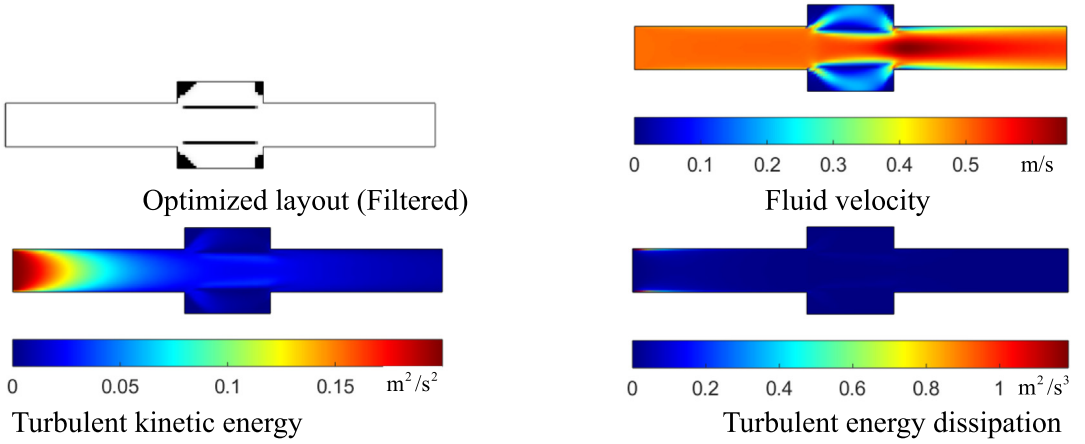

(a) $k_0 = 1.93\times10^{-3}$ m^2/s^2 and $\varepsilon_0 = 1.93\times10^{-5}$ m^2/s^3, objective function=82.9013×10^{-4} m^4/s^2

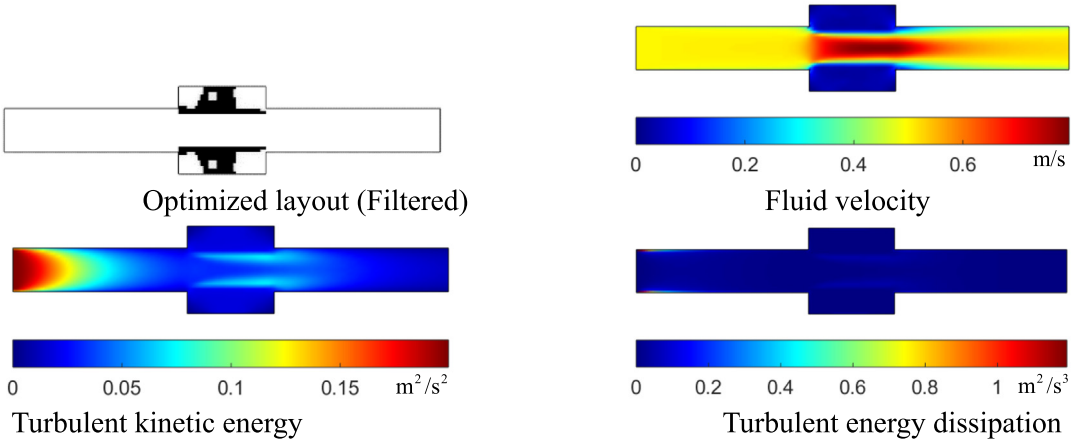

(b) $k_0 = 1.93\times10^{-2}$ m^2/s^2 and $\varepsilon_0 = 1.93\times10^{-4}$ m^2/s^3, objective function=164.1168×10^{-4} m^4/s^2

Fig. 10. Effects of the absorption of the solid domain using different k_0 and ε_0 values.

mass ratio. The straight channel with some bypath flows can be an optimized layout for the optimization problem described above as some folded designs inside the design domains can generate complex vortices and wakes in the channel, thus increasing the turbulent kinetic energy at the objective domain. Interestingly, there are the slits in the front and the rear of the straight structures that induce some detoured flows suppressing the flow motions in the y-direction. It seems that owing to these flows in the y-direction, some smooth flows can be obtained within the objective domain that can minimize the turbulent kinetic energy. It should be mentioned that the reason for the definition of the design domain with a center narrow channel attributed to a structure blocking channel should be the best design because there is no accumulation of turbulent kinetic energy without flow. Fig. 8 shows a porous design with an extended design domain blocking the channel after 14 iterations. The ill-posed condition occurs, i.e., an input and almost zero-output flow conditions apply through the porous membrane, thus yielding an increased velocity whose order is inversely proportional to the area of the porous material. Correspondingly, the material interpolation function and the analysis procedure fail to elicit a numerical solution, and the optimization process stops. When some numerical difficulties are observed, it may be possible to continue the optimization by decreasing the Reynolds number, i.e., increasing the viscosity for a few optimization iterations or increasing the number of mesh elements. However, these numerical treatments do not help here because the optimizer will encounter another blocking structure again and the numerical solution procedure will fail again to reach a numerical solution. Fig. 9

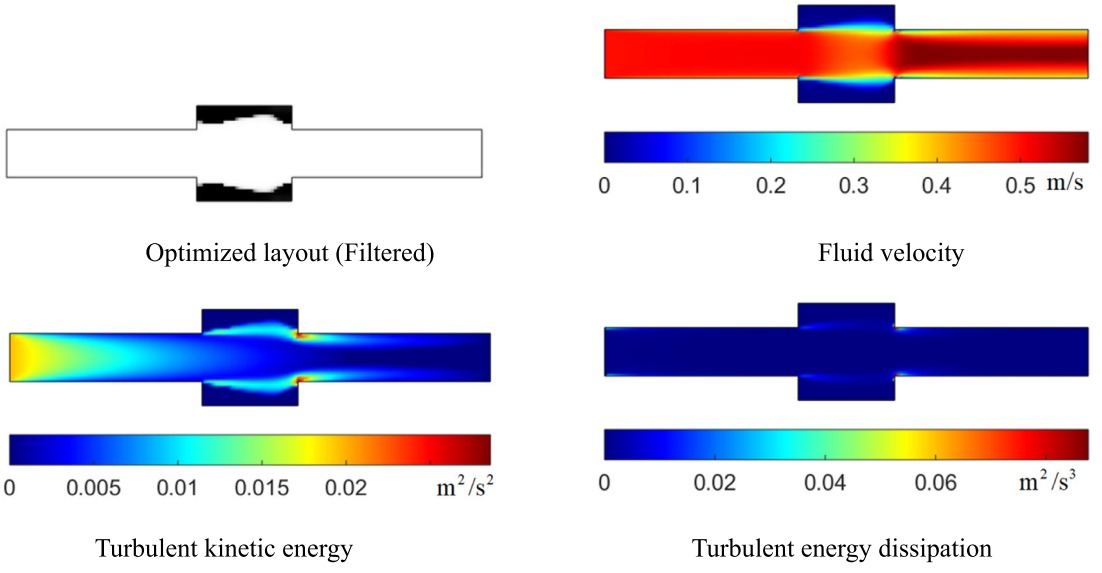

Fig. 11. Input boundary condition test subject to the constraint ($V_{Solid} = \int_{\Omega}(1-\gamma)d\Omega \geq V^0$, $k_{in} = 0.019$ m^2/s^2 :1/10 of the turbulent kinetic energy and $\varepsilon_{in} = 1.98 \times 10^{-3}$ m^2/s^3, objective function $= 6.5165 \times 10^{-4}$m^4/s^2, $V^0 = 50\%$) (remark: the fluid design is filled with fluid as an optimum configuration (zero-mass usage) with the mass constraint $V_{Solid} = \int_{\Omega}(1-\gamma)d\Omega \leq V^0$).

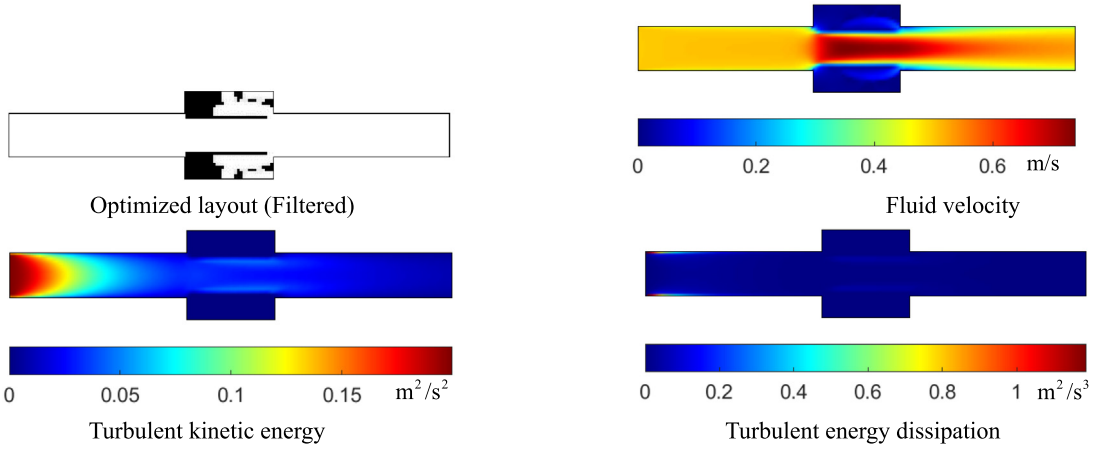

Fig. 12. Optimized layouts with turbulent energy dissipation (objective function $= 18.8554$ m^4/s^3).

shows the optimize design with a refined mesh (mesh size $= 0.015625$ m $\times$ 0.015625 m). The overall details are similar to the design with the coarse mesh in Fig. 6 with some curved surfaces along the structure. In this first example, the Kolmogorov length scale or the smallest length eddy scale is ($\eta = \left(v^3/\varepsilon\right)^{1/4} \sim 0.001$ m) and the approximate turbulent energy dissipation is ($\sim 0.5^3/10$). Therefore, with the DNS method, the minimum number of mesh in the x-direction (N) should be larger than $N = (\mathrm{Re})^{3/4}$. However, in the RANS simulation, the mesh discretization in the x-direction is 160 in Fig. 5 and 640 in Fig. 9.

Boundary Condition Test

Note that at a given Reynolds number, the drag of a turbulent flow is higher than the drag of a laminar flow owing to the transportation of the mechanical dynamic energy and its use for the creation of turbulent eddies of all sizes. Additionally, the turbulence absorption affects the turbulent flow and the drag force. Up to this point, the walls of the channels and channels are assumed to be smooth. Furthermore, in any turbulent flow, some unavoidable perturbations in initial conditions, boundary conditions, material properties, and turbulent flow, are extremely sensitive to these

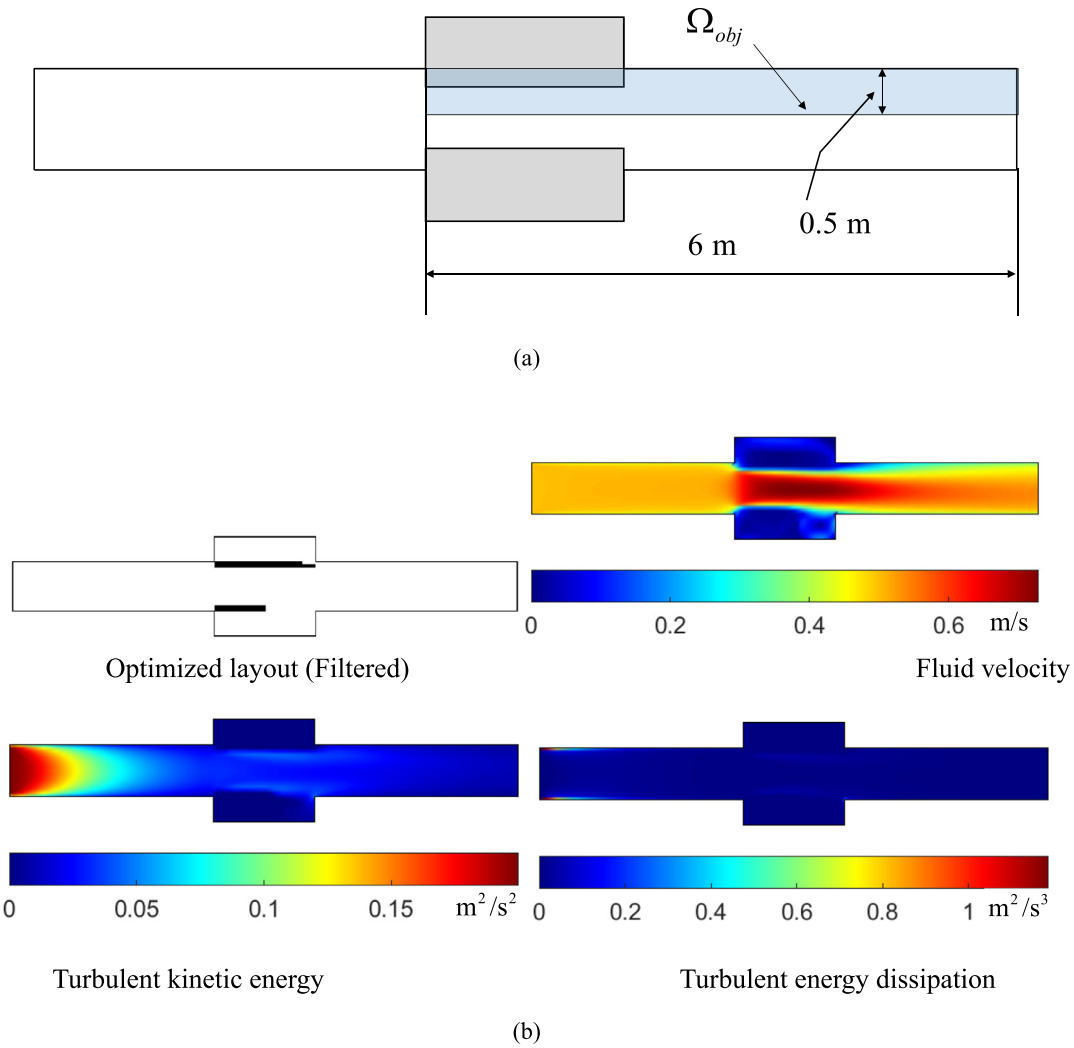

Fig. 13. Asymmetrical optimization with turbulent energy dissipation. (a) Problem definition and (b) optimized design.

perturbations. Thus, it is necessary to investigate the effect of the coefficients used to simulate the solid surface in (11) and (12). In the above example, we set zeros for the kinetic and the dissipation energy in (11) and (12). In order to test the effect of the roughness of the solid domain, different values can be tested in Fig. 10. As illustrated, straight designs, different objective function values can be obtained.

In addition to the boundary condition of the solid domain, the boundary condition of the input flow is also tested in Fig. 11. Correspondingly, the optimization is carried out in Fig. 11 using the same conditions except for the magnitudes and intensities of the kinetic and the dissipation energy. By decreasing the magnitude of the energies (1/10 of the kinetic energy in Fig. 5), the development of the energies in the middle domain becomes a dominant source. Interestingly, we have filled the fluid design with fluid as an optimum configuration (zero-mass usage) based on the constraint $V_{Solid} = \int_{\Omega}(1-\gamma)d\Omega \leq V^0$. It is our postulation that with a large turbulent kinetic energy in Fig. 6 the turbulent input influences the fluid motion at the middle domain, and the channel structure minimizes the objective function, or the turbulent kinetic energy appears in the objective domain. To avoid this condition, we changed the constraint type from a less-than to a greater-than condition, and the expansion chamber design could thus be obtained exemplifying the complexities and importance of the boundary conditions in the optimum design.

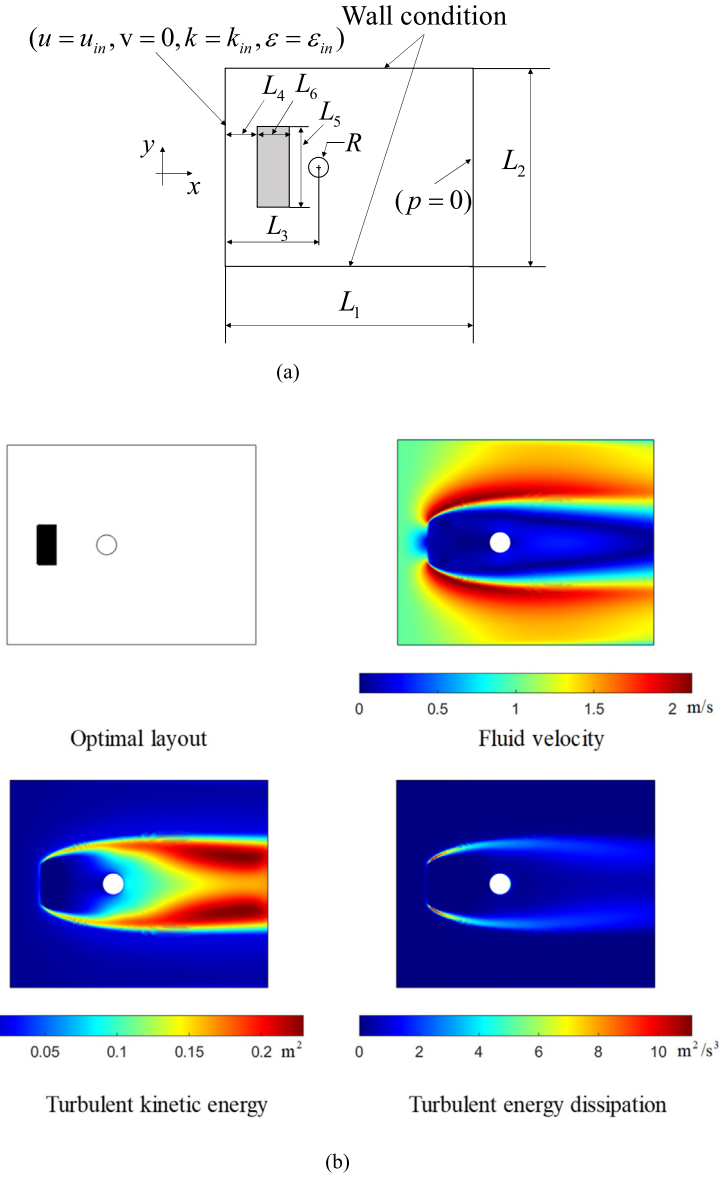

Fig. 14. Channel design with a hole (a) the problem definition (Air: $\rho = 1.25\,\text{kg/m}^3$, kinematic viscosity $= 1.42 \times 10^{-5}\text{Pa} \cdot \text{s}$, $L_{RE} = 0.5\,\text{m}$, $u_{in} = 1\,\text{m/s}$, Re $= 44\,014$ (Re $= \frac{\rho u L_{\text{RE}}}{\mu} = \frac{1.25\times1\times0.5}{1.42\times10^{-5}}$), $R = 0.02$ m, $k_{in} = 0.0056\ \text{m}^2/\text{s}^2$ and $\varepsilon_{in} = 1.2393 \times 10^{-4}\text{m}^2/\text{s}^3$, V^0:30%, $L_1 = 0.5\,\text{m}$, $L_2 = 0.4\,\text{m}$, $L_3 = 0.2\,\text{m}$, $L_4 = 0.06\,\text{m}$, $L_5 = 0.08\,\text{m}$, $L_6 = 0.04\,\text{m}$) and (b) a solid initial design (Objective: 0.0113 m^4/s^2).

Some isolated dots in the chambers appear due to the local optimum issue; they appear at the beginning of the optimization and they do remain.

Optimization with the turbulent energy dissipation

It is also possible to consider the turbulent energy dissipation in the same objective domain in Fig. 12. There are prior research studies that have considered the kinetic and the dissipation energy in the analysis/shape optimization for turbulent flow in order to reduce the side effects of the turbulent flow. For example, in [59] and some references therein, flow-induced noise from CFD analysis was modeled with the kinetic and the dissipation energy. Using the developed optimization procedure, we could obtain a similar straight line layout expected by the consideration of the transportation equations in (11) and (12). Comparing the terms of the equations, some similarity can be found

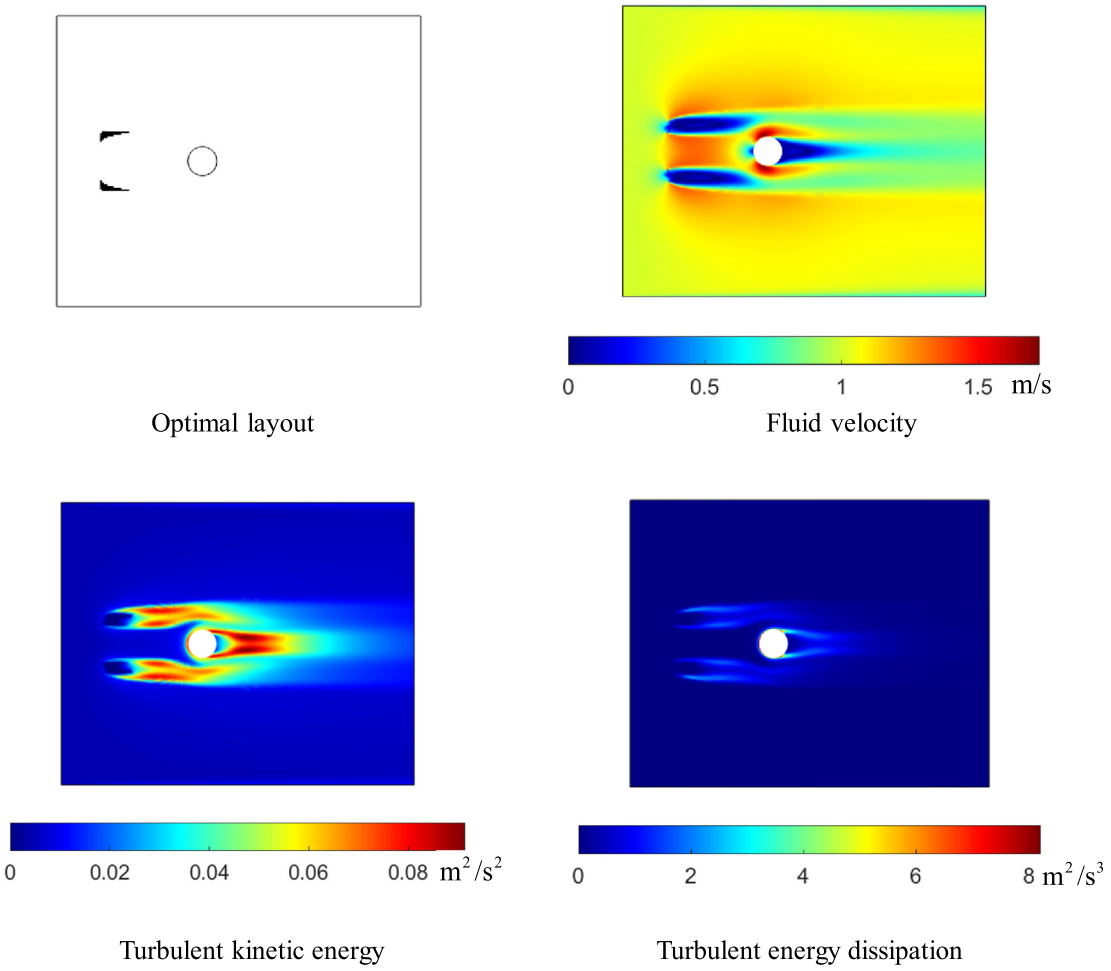

Fig. 15. An optimized design minimizing the turbulent kinetic energy over the domain with 30% mass (Objective: 0.0026 m^4/s^2).

with some differences in the constants multiplied by the source term and the dissipation terms.

$$\begin{aligned} &\text{Minimize } \phi = \int_{\Omega_{obj}} \varepsilon d\Omega \\ &\text{Subject to } V_{Solid} = \int_{\Omega} (1-\gamma) d\Omega \leq V^0 \end{aligned} \tag{19}$$

In Fig. 13, the nonsymmetrical objective domain is considered with the optimization formulation of (19). The objective domain is defined at the upper part of the analysis domain. The design of Fig. 13(b) shows a straight line and a slope in the bottom domain to minimize the dissipation domain at the upper domain.

Example 2: Channel with a hole

For the next numerical example, the channel with a hole in Fig. 14 is considered. A block is placed in front of the hole and is set to the design domain. Air flow moved from the left side to the right side with a velocity inside the channel of 1 m/s. Then the optimization formulation is to minimize the integral of the turbulent kinetic energy over the overall domain with the 30% mass constraint. As a reference and an initial design, the solid box is considered in Fig. 14(b) and its objective function was 0.0113 m^4/s^2. With the solid box, the flow is separated at the box and the most of the turbulent kinetic energy is observed after the hole. With the application of the present topology optimization, the nozzle shape design with 0.0026 m^4/s^2 of the turbulent kinetic energy in Fig. 15 can be obtained. The distribution of the fluid velocity shows that the fluid is divided into three parts and the smaller

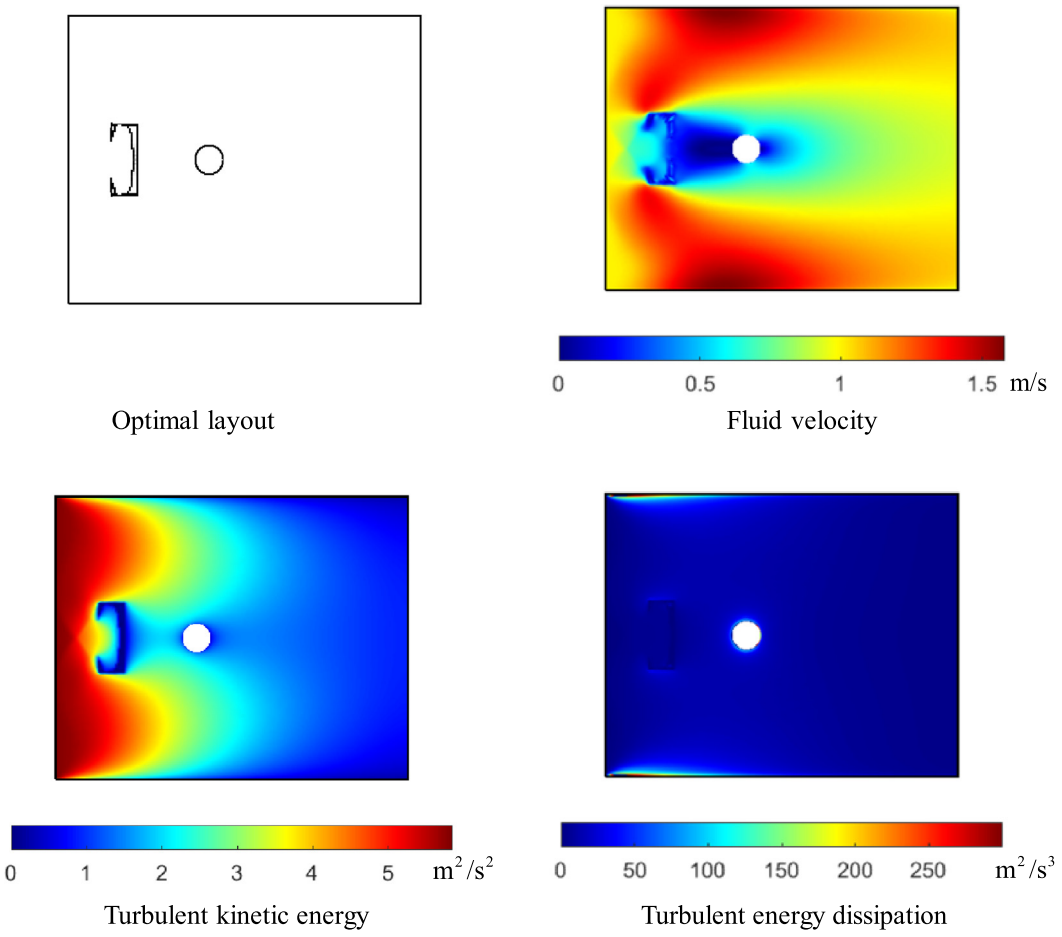

Fig. 16. The other optimized design with the different input condition ($k_{in} = 5.6$ m^2/s^2, Objective: 0.4596 m^4/s^2).

turbulent kinetic energy appears. The two bodies in Fig. 14(b) separate the fluid and this increases the turbulent kinetic energies as well as the turbulent dissipation before the hole. It seems it works as a nozzle which increases the fluid velocity. As a result, the overall turbulent kinetic energy in Fig. 15 is smaller than that in Fig. 14(b).

For the next example, the turbulent kinetic energy is artificially increased by 1000 times to consider the effect of the boundary condition. Due to the boundary condition, the objective values of solid and fluid designs become 0.4550 m^4/s^2 and 0.6061 m^4/s^2; the solid design is preferred. With the same condition except the boundary condition, the optimized design Fig. 16 can be obtained. This example again shows that the optimized layouts of topology optimization problems considering the effect of turbulence are influenced by the boundary condition and the problem definition.

Example 3: Fluid path design

For the next numerical example, an optimized design of the L-shape channel in Fig. 17 is considered. The fluid flows from the left side to the channels at the upper side. It was assumed that air flow moved from the left side to the right upper open side with a velocity inside the channel of 0.5 m/s. In this system, the fluid flow exhibits complex movements at the corner and after the corner (recirculation and reattach) and we observe the higher turbulent kinetic energy after the corner. In consideration of some engineering-related applications, i.e., maintenance, noise control, or corrosion prevention, we want to minimize the turbulent kinetic energy at the right upper part of the channel. One of the obvious designs may be the blocking the fluid, i.e., no flow and no turbulent kinetic energy but some drains should also be considered. Therefore, the consideration of the turbulent kinetic energy only is improper to make a channel and the considering the fluid dissipated energy ($\dot{E}_{fludic}$) is necessary. For this reason, the adjacent domain

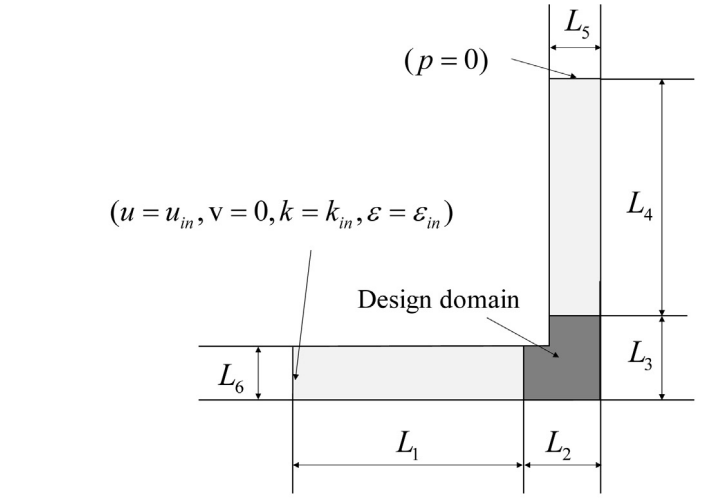

(a)

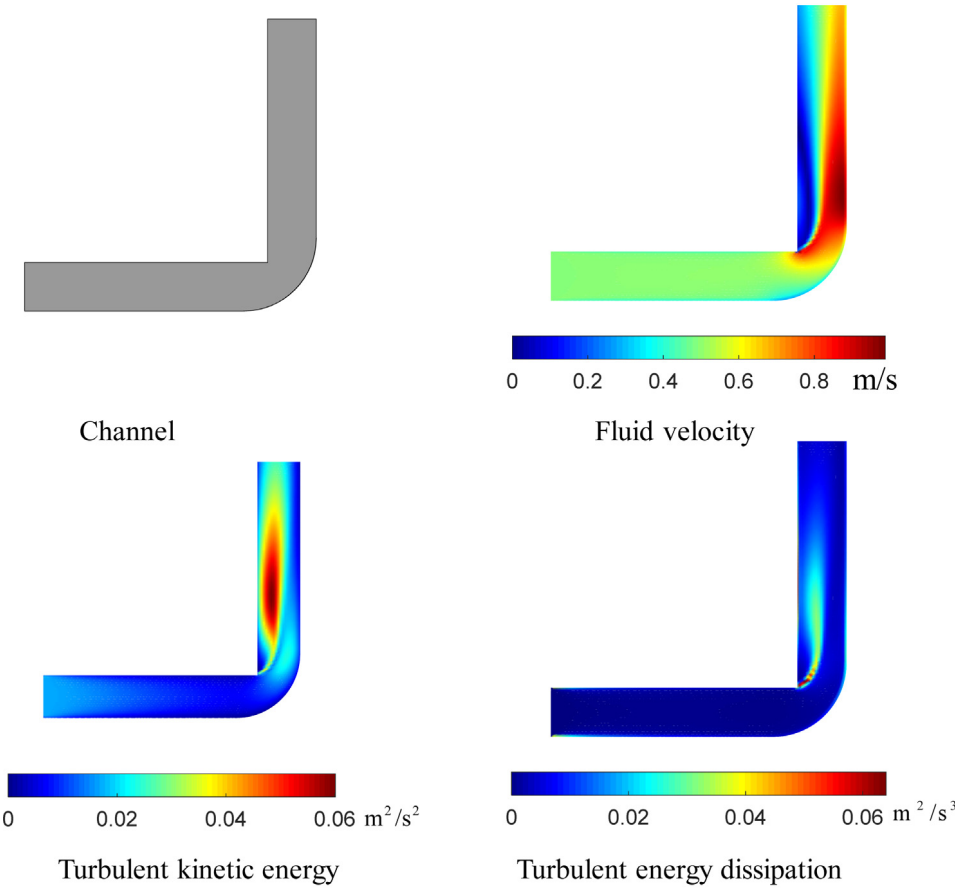

(b)

Fig. 17. (a) L-shaped fluid channel design (Air: $\rho = 1.25\,\mathrm{kg/m^3}$, kinematic viscosity $= 1.42 \times 10^{-5}\mathrm{Pa \cdot s}$, $L_{RE} = 1\,\mathrm{m}$, $u_{in} = 0.5\,\mathrm{m/s}$, Re $= 4.4014 \times 10^4$(Re $= \frac{\rho u L_{\mathrm{RE}}}{\mu} = \frac{1.25 \times 0.5 \times 1}{1.42 \times 10^{-5}}$), $L_1 = 4.5\,\mathrm{m}$, $L_2 = 1.5\,\mathrm{m}$, $L_3 = 1.5\,\mathrm{m}$, $L_4 = 4.5\,\mathrm{m}$, $L_5 = 1\,\mathrm{m}$, $L_6 = 1\,\mathrm{m}$, $k_{in} = 0.019\ \mathrm{m^2/s^2}$ and $\varepsilon_{in} = 1.98 \times 10^{-5}\mathrm{m^2/s^3}$, V^0:50%, Erode Morphological filter radius: 0.0938 m) and (b) the reference L-shape pipe with one side fillet with the 1.5 m radius (Turbulent kinetic energy: 0.2104 $\mathrm{m^4/s^2}$).

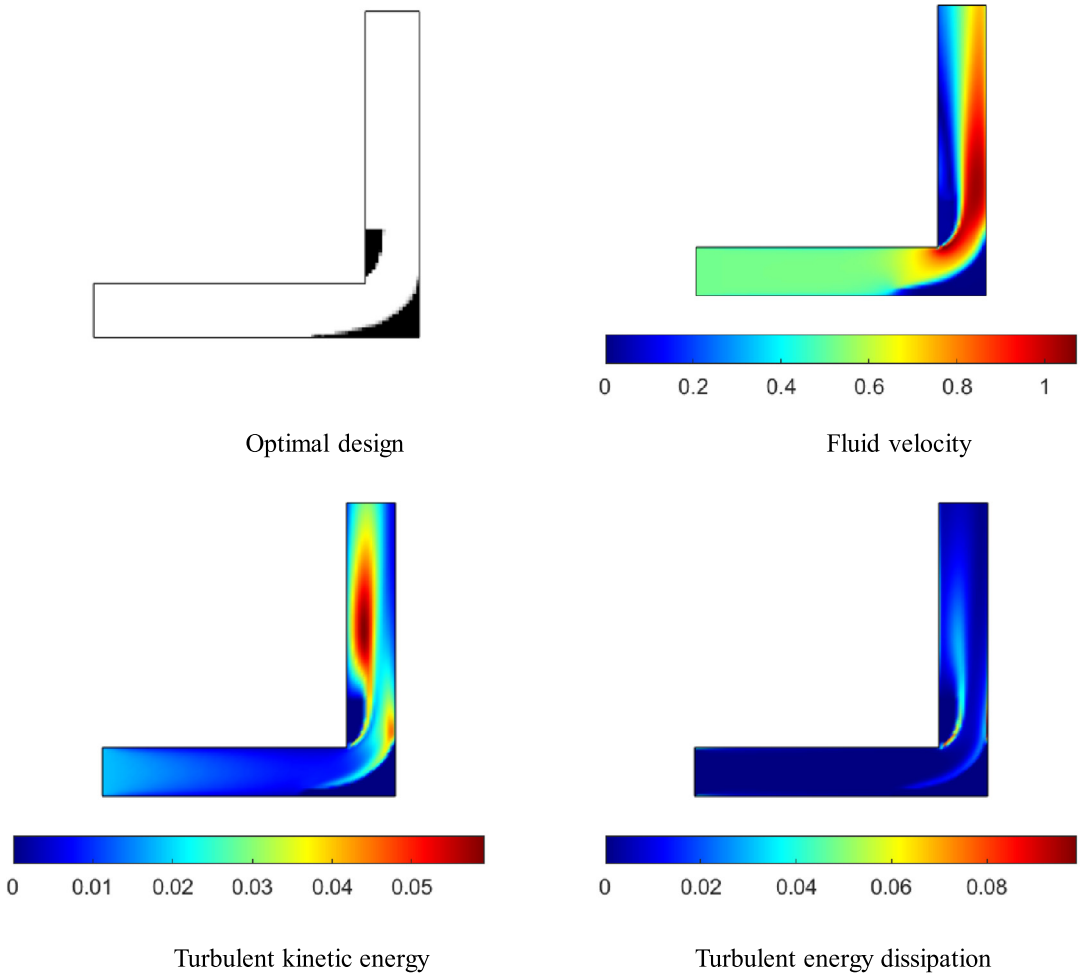

Fig. 18. An optimized design minimizing the dissipation only and the integral of the turbulent kinetic energy. (the integral of the turbulent kinetic energy: 0.2096 m^4/s^2, $\dot{E}_{fludic}$: 0.1132 $(Pa \cdot m^3/s)$).

of the corner is set to the design domain for the following optimization formulation in (20) with the combination of the integrals of the turbulent kinetic energy at the analysis domain subject to the constraints of the turbulent energy dissipation at the analysis domain and the mass constraint. The upper bound of the integration of the turbulent energy dissipation is denoted by $\widetilde{E}_{fludic}$ which is set to the two times of the turbulent energy dissipation of the fluid pipe, i.e., the turbulent energy dissipation of the fluid pipe, 0.0566 $(Pa \cdot m^3/s)$. Without the constraint of the turbulent energy dissipation, a blocking structure appears. In the channel design in Fig. 17(b), the fluid passes and turns at the sharp corner and the higher turbulent kinetic is observed. With the topology optimization, the curve shape channel is obtained with the turbulent kinetic energy with 0.2096 m^4/s^2. Compared with the turbulent kinetic energy of the curved pipe shown in Fig. 17(b) with 0.2104 m^4/s^2, i.e., the integration of the turbulent energy is lower (see Fig. 18).

$$\begin{aligned} &\text{Minimize} \quad \int_{\Omega} k d\Omega \\ &\text{Subject to} \quad \int_{\Omega} \gamma d\Omega \leq V^0 \\ &\qquad\qquad \dot{E}_{fludic} \leq \tilde{E}_{fludic} \end{aligned} \tag{20}$$

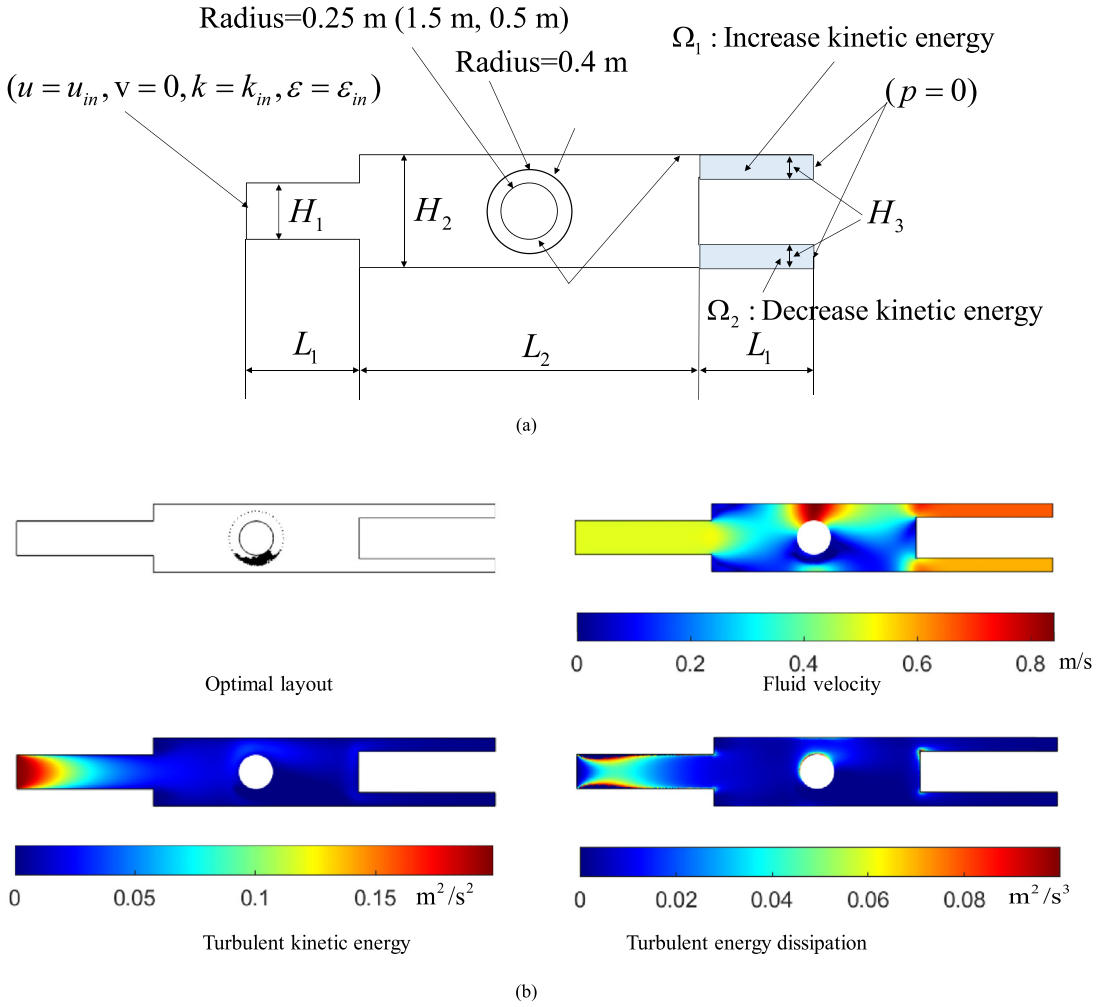

Fig. 19. Fluid separator design. (a) A problem definition ($k_{in} = 0.19$ m^2/s^2 and $\varepsilon_{in} = 1.98 \times 10^{-5}$ m^2/s^3, maximum element size $= 0.01$ m) and (b) an optimized design with 30% mass ($\int_{\Omega_1} k d\Omega = 0.0022506$ m^4/s^2, $\int_{\Omega_2} k d\Omega = 0.0013898$ m^4/s^2) and their velocity, turbulent kinetic energy and turbulent energy dissipation ($\varepsilon < 0.01$ m^2/s^3).

$$\dot{E}_{fludic} = \int_{\Omega} \frac{1}{2}(\mu + \mu_T)\left(\nabla \mathbf{u} + \nabla \mathbf{u}^T\right) : \left(\nabla \mathbf{u} + \nabla \mathbf{u}^T\right) + \alpha \mathbf{u} \cdot \mathbf{u} d\Omega (\text{Pa} \cdot \text{m}^3/\text{s}) \tag{21}$$

Example 4: Controlling the turbulent kinetic energy

For the final numerical example, an optimized fluid separator with a hole is considered in Fig. 14. The fluid flows from the left side to the channels at the right side. In the analysis domain, we assume that a hole is placed at the center. Due to this inclusion of the hole, the fluid flow shows complex movements. To consider some engineering purposes, i.e., maintenance issue, noise control, or corrosion prevent, we want to minimize the turbulent kinetic energy at the right bottom pipe. One of the obvious designs may be the blocking the right bottom pipe but some drains are also considered. For this reason, the adjacent domain of the hole is set to the design domain for the following optimization formulation with the simple combinations of the integrals of the kinetic energy at the two pipes with the mass constraint. All the examples use the quadrilateral elements and the triangular elements as shown in Fig. 1 and we employ the triangular mesh for this problem. It is assumed that air flow moves from the left side to the right open side with 0.5 m/s velocity inside the channel with 10 m ($L_1 = 2$ m, $L_2 = 3$ m, $H_1 = 1$ m , $H_2 = 1$ m). Based on the material properties and the lengths, the estimate Reynolds number is again about 4.4014×10^4 ($L_{\text{RE}} = 1$ m, $\text{Re} = \frac{\rho u L_{\text{RE}}}{\mu} = \frac{1.25 \times 0.5 \times 1}{1.42 \times 10^{-5}}$) that shows the turbulent flow. The following optimization problem in

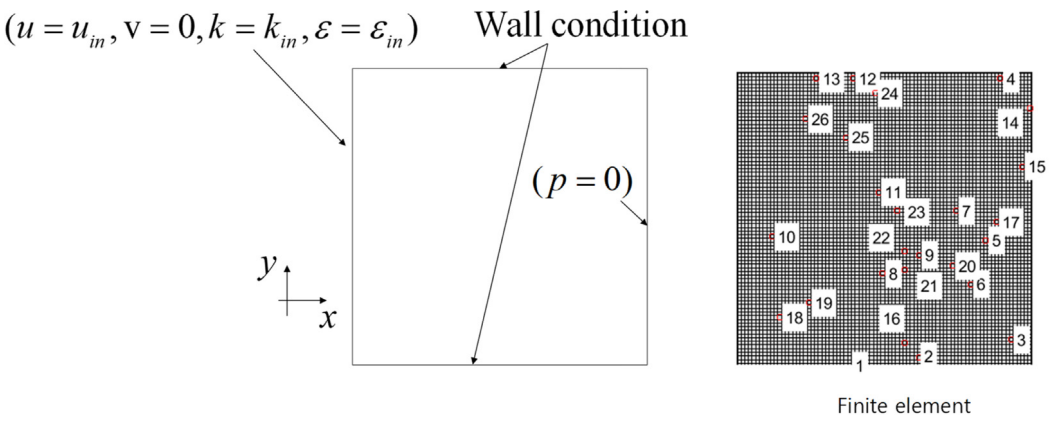

(a)

Element	FDM (perturbation=1e-3)	Adjoint	Error (Percentage)
1	-1.61E-05	-1.56E-05	3.21
2	-4.29E-06	-4.12E-06	4.05
3	-2.31E-07	-1.85E-07	24.74
4	-3.16E-06	-3.17E-06	0.32
5	3.43E-07	3.20E-07	7.17
6	8.57E-07	8.20E-07	4.57
7	2.64E-07	2.40E-07	10.19
8	1.44E-06	1.33E-06	8.25
9	5.87E-07	5.39E-07	8.92
10	9.33E-07	8.34E-07	11.80
11	7.58E-07	6.89E-07	10.02
12	-1.29E-05	-1.24E-05	4.23
13	-1.53E-05	-1.43E-05	6.71
14	6.31E-08	9.96E-08	36.66
15	6.42E-07	6.20E-07	3.46
16	6.14E-07	7.90E-07	22.33
17	3.07E-07	2.86E-07	7.33
18	4.14E-06	3.74E-06	10.63
19	3.84E-06	3.51E-06	9.42
20	6.21E-07	5.81E-07	6.84
21	1.05E-06	9.74E-07	7.98
22	6.18E-07	5.64E-07	9.49
23	4.18E-07	3.75E-07	11.62
24	-7.01E-07	-3.96E-07	76.90
25	3.49E-06	3.23E-06	8.22
26	4.73E-06	4.34E-06	8.91

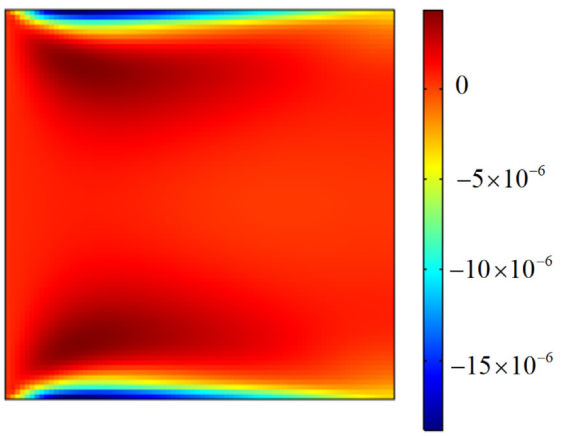

(b)

Fig. 20. The sensitivity analysis 1. (a) The problem definition ($u_{in} = 1\,\mathrm{m/s}, k_{in} = 4.8513 \times 10^{-3}\mathrm{m}^2/\mathrm{s}^2$, $\varepsilon_{in} = 7.9818 \times 10^{-5}\,\mathrm{m}^2/\mathrm{s}^3$, $l = 1$ m, Air: $\rho = 1.25\,\mathrm{kg/m}^3$, kinematic viscosity $= 1.42 \times 10^{-5}\mathrm{m}^2/\mathrm{s}$) (b) the sensitivity comparison of the integration of the turbulent kinetic energy and (c) the sensitivity comparison of the integration of the turbulent energy dissipation.

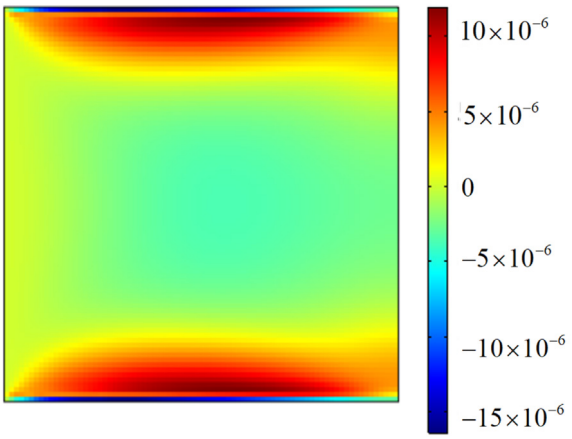

Element	FDM	Adjoint	Error (Percentage)
1	-1.45E-05	-1.56E-05	0.92
2	1.23E-05	1.19E-05	1.03
3	3.97E-06	3.79E-06	1.05
4	5.16E-06	5.50E-06	0.94
5	-2.82E-06	-2.83E-06	1.00
6	-2.04E-06	-1.92E-06	1.06
7	-3.21E-06	-3.23E-06	0.99
8	-3.21E-06	-2.95E-06	1.09
9	-3.42E-06	-3.35E-06	1.02
10	-7.56E-07	-5.90E-07	1.28
11	-3.52E-06	-3.41E-06	1.03
12	7.55E-06	6.47E-06	1.17
13	7.36E-06	5.81E-06	1.27
14	3.28E-06	3.17E-06	1.03
15	-1.82E-06	-1.76E-06	1.03
16	8.17E-06	7.82E-06	1.04
17	-2.80E-06	-2.82E-06	0.99
18	-3.61E-07	1.81E-07	-2.00
19	-1.39E-06	-7.80E-07	1.78
20	-2.90E-06	-2.82E-06	1.03
21	-3.27E-06	-3.09E-06	1.06
22	-3.52E-06	-3.45E-06	1.02
23	-3.61E-06	-3.59E-06	1.01
24	9.76E-06	9.21E-06	1.06
25	-1.43E-06	-8.40E-07	1.70
26	7.29E-07	1.30E-06	0.56

Fig. 20. (*continued*).

(20) is considered. Due to the symmetric condition, the objective function of fluid-filled design is zero. Fig. 19(b) shows an optimized design. With the boundary condition with a large input turbulent kinetic energy, the topology optimization scheme finds out an optimized layout to block the fluid input to the lower arm. With the optimized design, the increases of the velocity, the turbulent kinetic energy and the energy dissipation above the hole can be observed.

$$\begin{aligned} &\text{Minimize } \int_{\Omega_2} k d\Omega - \int_{\Omega_1} k d\Omega \\ &\text{Subject to } V_{Solid} = \int_{\Omega} (1-\gamma) d\Omega \leq V^0 \end{aligned} \tag{22}$$

4. Conclusions

The present study developed a new TO for turbulent flow based on the k–ε turbulent model without the frozen turbulence assumption. In the Reynolds–averaged Navier–Stokes (RANS) equation for turbulent flow, we considered the eddy viscosity value computed by the transportation equations to the Navier–Stokes equation. With the proper boundary conditions, the average turbulent flow could be obtained by solving the Reynolds–averaged Navier–Stokes equations. For topology optimization, the Navier–Stokes equation and the transportation equations were modified with respect to the spatially varying design variables. We intended to show that the present approach is a good compromise in terms of the simplicity of the topology optimization for turbulent flow. The present study considered the effects of the turbulent flow in the objective function and the associated constraints. In conclusion, this research developed a new topology optimization scheme for the k–ε turbulent model based on finite elements. The effects

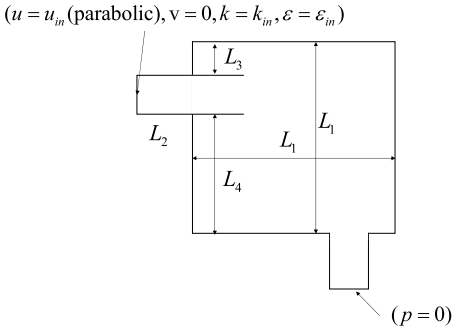

(a) Domain

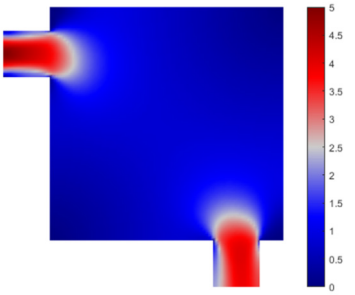

(b) Fluid velocity

Element order	FDM	Sensitivity	Error (Percentage)
1	-2.2327E-03	-2.2305E-03	0.0982
2	-8.5814E-04	-8.7028E-04	1.3952
3	-3.3818E-04	-3.4490E-04	1.9465
4	-1.9957E-04	-2.0039E-04	0.4107
5	-1.3239E-04	-1.3261E-04	0.1726
6	-9.0404E-05	-9.0500E-05	0.1066
7	-6.0850E-05	-6.0936E-05	0.1407
8	-3.9168E-05	-3.9343E-05	0.4452
9	-2.3952E-05	-2.4157E-05	0.8499
10	-1.5172E-05	-1.5095E-05	0.5074

Fluid dissipation energy

Element order	FDM	Sensitivity	Error (Percentage)
1	9.1391E-05	9.2202E-05	0.8796
2	7.6422E-05	7.7008E-05	0.7607
3	7.0782E-05	7.4403E-05	4.8676
4	7.3779E-05	7.2044E-05	2.4071
5	6.5833E-05	6.9929E-05	5.8570
6	6.6738E-05	6.8400E-05	2.4309
7	6.7105E-05	6.7240E-05	0.2010
8	6.9199E-05	6.6368E-05	4.2659
9	6.7862E-05	6.5484E-05	3.6318
10	5.9383E-05	6.4694E-05	8.2100

Turbulent kinetic energy

Element order	FDM	Sensitivity	Error (Percentage)
1	3.1453E-05	3.2585E-05	3.4740
2	2.7210E-05	2.8301E-05	3.8564
3	2.5852E-05	2.7322E-05	5.3810
4	2.5354E-05	2.6783E-05	5.3332
5	2.5254E-05	2.6352E-05	4.1687
6	2.5155E-05	2.6615E-05	5.4881
7	2.5023E-05	2.6148E-05	4.2998
8	2.4898E-05	2.5383E-05	1.9106
9	2.4797E-05	2.5742E-05	3.6716
10	2.4723E-05	2.5229E-05	2.0066

Turbulent dissipation energy

(c)

Fig. 21. The sensitivity analysis 2. (a) The problem definition (Initial density=0.9, $u_{in} = 5\,\text{m/s}$, $k_{in} = 0.4459\ \text{m}^2/\text{s}^2$, $\varepsilon_{in} = 0.069822\ \text{m}^2/\text{s}^3$, $L_1 = 1$ m, $L_2 = 0.2$ m, $L_3 = 0.1$ m, $L_4 = 0.7$ m, Air:$\rho = 1.25\,\text{kg/m}^3$, kinematic viscosity $= 1.42 \times 10^{-5}\text{m}^2/\text{s}$, (b) the fluid velocity and (c) the comparison of the sensitivity.

of the turbulent flow were investigated based on the solution of several practical problems. For future research, it is important to compare the RANS models for a specific condition and compare the numerical results with the experimental results to choose a proper RANS model. After that, the modifications of the RANS model for topology optimization should be followed.

Acknowledgments

This work was supported by the National Research Foundation of Korea (NRF) grant funded by the Korea government (MSIT) (No. NRF-2019R1A2C2084974).

Appendix. The sensitivity analysis

The present study adopts the adjoint sensitivity analysis to compute the sensitivity values of the objective values. To check the accuracy, we consider the rectangular domain in Fig. 20 and compare the sensitivity values of the finite difference method and the adjoint sensitivity analysis. With very small values of the finite difference method, the errors become relative large due to the numerical errors.

For the second sensitivity analysis example with the fluid dissipation energy, turbulent kinetic energy and turbulent dissipation energy, the sensitivity analysis of the box problem in Fig. 21 is considered. As the sensitivity analysis assumes zero for the residual of the governing equation, it is important to obtain the accurate solution.

References

[1] S. Pope, Turbulent Flows, Cambridge University Press, Cambridge, 2000.

[2] E.M. Papoutsis-Kiachagias, E.A. Kontoleontos, A.S. Zymaris, D.I. Papadimitriou, K.C. Giannakoglou, Constrained topology optimization for laminar and turbulent flows, including heat transfer, in: Proc. EUROGEN, Evolutionary and Deterministic Methods for Design, Optimization and Control, Capua, Italy, 2011.

[3] G.H. Yoon, Topology optimization for turbulent flow with Spalart–Allmaras model, Comput. Method Appl. Mech. 303 (2016) 288–311.

[4] E. Oktay, H.U. Akay, O. Merttopcuoglu, Parallelized structural topology optimization and CFD coupling for design of aircraft wing structures, Comput. & Fluids 49 (2011) 141–145.
[5] E.A. Kontoleontos, E.M. Papoutsis-Kiachagias, A.S. Zymaris, D.I. Papadimitriou, K.C. Giannakoglou, Adjoint-based constrained topology optimization for viscous flows, including heat transfer, Eng. Optim. 45 (2013) 941–961.
[6] B.J. Lee, C. Kim, Automated design methodology of turbulent internal flow using discrete adjoint formulation, Aerosp. Sci. Technol. 11 (2007) 163–173.
[7] K.J. Bathe, H. Zhang, A mesh adaptivity procedure for CFD and fluid–structure interactions, Comput. Struct. 87 (2009) 604–617.
[8] T. Javaherchi, Review of Spalart–Allmaras Turbulence Model and its Modifications, University of Washington, ME Department, 2011.
[9] A. Crivellini, V. D'Alessandro, Spalart–Allmaras model apparent transition and RANS simulations of laminar separation bubbles on airfoils, Int. J. Heat Fluid Flow 47 (2014) 70–83.
[10] C. Rumsey, The Spalart–Allmaras turbulence model, in: Webpage at Langley Research Center, Langley Research Center.
[11] C.D. Argyropoulos, N.C. Markatos, Recent advances on the numerical modelling of turbulent flows, Appl. Math. Model. 39 (2015) 693–732.
[12] D.C. Wilcox, Turbulence Modeling for CFD, third ed., DCW Industries, La Cãnada, Calif., 2006.
[13] ANSYS, Introduction to analysis fluent, Customer Training Material.
[14] OPENFOAM, Turbulence models, 2014, http://www.openfoam.org/features/turbulence.php.
[15] M. Bendsœ, O. Sigmund, Topology Optimization : Theory, Methods, and Applications, Springer, Berlin, New York, 2003.
[16] A. Bueno-Orovio, C. Castro, F. Palacios, E. Zuazua, Continuous adjoint approach for the Spalart–Allmaras model in aerodynamic optimization, AIAA J. 50 (2012) 631–646.
[17] A.S. Zymaris, D.I. Papadimitriou, K.C. Giannakoglou, C. Othmer, Continuous adjoint approach to the Spalart–Allmaras turbulence model for incompressible flows, Comput. & Fluids 38 (2009) 1528–1538.
[18] C.B. Dilgen, S.B. Dilgen, D.R. Fuhrman, O. Sigmund, B.S. Lazarov, Topology optimization of turbulent flows, Comput. Method Appl. Mech. 331 (2018) 363–393.
[19] Z.L. Han, D. Zhou, J.H. Tu, C.Q. Fang, T. He, Flow over two side-by-side square cylinders by CBS finite element scheme of Spalart–Allmaras model, Ocean Eng. 87 (2014) 40–49.
[20] P.R. Spalart, S.R. Allmaras, A one-equation turbulence model for aerodynamic flows, Rech. Aerosp. 1 (1994) 5–21.
[21] P.R. Spalart, Strategies for turbulence modelling and simulations, Int. J. Heat Fluid Flow 21 (2000) 252–263.
[22] F.M. White, Fluid Mechanics, McGraw Hill International ed., 1994.
[23] R. David, T. Florist, On the nature of turbulence, Commun. Math. Phys. 20 (1971) 167–192.
[24] N.A. Adams, Direct numerical simulation of turbulent compression ramp flow, Theor. Comput. Fluid Dyn. 12 (1998) 109–129.
[25] T. Borrvall, J. Petersson, Topology optimization of fluids in Stokes flow, Internat. J. Numer. Methods Fluids 41 (2003) 77–107.
[26] M. Bruggi, P. Venini, Topology optimization of incompressible media using mixed finite elements, Comput. Method Appl. Mech. 196 (2007) 3151–3164.
[27] G.H. Yoon, J.S. Jensen, O. Sigmund, Topology optimization of acoustic-structure interaction problems using a mixed finite element formulation, Internat. J. Numer. Methods Engrg. 70 (2007) 1049–1075.
[28] G.H. Yoon, Unified analysis with mixed finite element formulation for acoustic-porous-structure multiphysics system, J. Comput. Acoust. 23 (2015).
[29] L.F.N. Sá, J.S. Romero, O. Horikawa, E.C.N. Silva, Topology optimization applied to the development of small scale pump, Struct. Multidiscip. Optim. 57 (2018) 2045–2059.
[30] A. Evgrafov, G. Pingen, K. Maute, Topology optimization of fluid domains: kinetic theory approach, ZAMM - J. Appl. Math. Mech. 88 (2008) 129–141.
[31] S. Zhou, Q. Li, A variational level set method for the topology optimization of steady-state Navier–Stokes flow, J. Comput. Phys. 227 (2008) 10178–10195.
[32] K. Yonekura, Y. Kanno, A flow topology optimization method for steady state flow using transient information of flow field solved by lattice Boltzmann method, Struct. Multidiscip. Optim. 51 (2015) 159–172.
[33] E.M. Papoutsis-Kiachagias, K.C. Giannakoglou, Continuous adjoint methods for turbulent flows, applied to shape and topology optimization: Industrial applications, Arch. Comput. Method Eng. (2014).
[34] P. Mirza, J. Hrvoje, R. Henrik, R. Christoph, RANS turbulence treatment for continuous adjoint optimization, in: Proc. 8th International Symposium on Turbulence, Heat and Mass Transfer, Sarajevo, Bosnia and Herzegovina, Vol. 8, 2015.
[35] A. Jemcov, D. Stephens, Topological derivatice formulation for shape sensitivity in incompressible turbulnet flow, in: Proc. Ninth International Conference on CFD in the Minerals and Process Industries, CSIRO, Melbourne, Australia, 2012.
[36] C. Othmer, Adjoint methods for car aerodynamics, J. Math. Ind. 4 (2014) 6.
[37] Y.B. Deng, Z.Y. Liu, Y.H. Wu, Topology optimization of steady and unsteady incompressible Navier–Stokes flows driven by body forces, Struct. Multidiscip. Optim. 47 (2013) 555–570.
[38] N. Jenkins, K. Maute, An immersed boundary approach for shape and topology optimization of stationary fluid–structure interaction problems, Struct. Multidiscip. Optim. 54 (2016) 1191–1208.
[39] G.H. Yoon, Topological design of heat dissipating structure with forced convective heat transfer, J. Mech. Sci. Technol. 24 (2010) 1225–1233.
[40] G.H. Yoon, Topological layout design of electro-fluid-thermal-compliant actuator, Comput. Method Appl. Mech. 209 (2012) 28–44.
[41] G.H. Yoon, Topology optimization for stationary fluid–structure interaction problems using a new monolithic formulation, Internat. J. Numer. Methods Engrg. 82 (2010) 591–616.
[42] R. Picelli, W.M. Vicente, R. Pavanello, Evolutionary topology optimization for structural compliance minimization considering design-dependent FSI loads, Finite Elem. Anal. Des. 135 (2017) 44–55.

[43] S. Deck, P. Duveau, P. d'Espiney, P. Guillen, Development and application of Spalart–Allmaras one equation turbulence model to three-dimensional supersonic complex configurations, Aerosp. Sci. Technol. 6 (2002) 171–183.
[44] A. Legay, J. Chessa, T. Belytschko, An Eulerian–Lagrangian method for fluid–structure interaction based on level sets, Comput. Method Appl. Mech. 195 (2006) 2070–2087.
[45] G.H. Yoon, Stress-based topology optimization method for steady-state fluid–structure interaction problems, Comput. Method Appl. Mech. 278 (2014) 499–523.
[46] Y.B. Deng, Z.Y. Liu, Y.S. Liu, Y.H. Wu, Combination of topology optimization and optimal control method, J. Comput. Phys. 257 (2014) 374–399.
[47] A. Gersborg-Hansen, O. Sigmund, R.B. Haber, Topology optimization of channel flow problems, Struct. Multidiscip. Optim. 30 (2005) 181–192.
[48] S. Kreissl, G. Pingen, A. Evgrafov, K. Maute, Topology optimization of flexible micro-fluidic devices, Struct. Multidiscip. Optim. 42 (2010) 495–516.
[49] D. Makhija, G. Pingen, R.G. Yang, K. Maute, Topology optimization of multi-component flows using a multi-relaxation time lattice Boltzmann method, Comput. & Fluids 67 (2012) 104–114.
[50] G. Pingen, K. Maute, Optimal design for non-Newtonian flows using a topology optimization approach, Comput. Math. Appl. 59 (2010) 2340–2350.
[51] E.M. Dede, Optimization and design of a multipass branching microchannel heat sink for electronics cooling, J. Electron. Packag. 134 (2012).
[52] E.M. Dede, J. Lee, Y. Liu, B. Robert, S.H. Yonak, Computational methods for the optimisation and design of electromechanical vehicle systems, Int. J. Veh. Des. 58 (2012) 159–180.
[53] S. Kreissl, G. Pingen, K. Maute, Topology optimization for unsteady flow, Internat. J. Numer. Methods Engrg. 87 (2011) 1229–1253.
[54] M. Ciofalo, M.W. Collins, k-ε Predictions of heat transfer in turbulent recirculating flows using an improved wall treatment, Numer. Heat Transfer B 15 (1989) 21–47.
[55] G. Söderlind, L. Wang, Adaptive time-stepping and computational stability, J. Comput. Appl. Math. 185 (2006) 225–243.
[56] L.H. Olesen, F. Okkels, H. Bruus, A high-level programming-language implementation of topology optimization applied to steady-state Navier–Stokes flow, Internat. J. Numer. Methods Engrg. 65 (2006) 975–1001.
[57] G.M. Lilley, The radiated noise from isotropic turbulence, Theor. Comp. Fluid Dyn. 6 (1994) 281–301.
[58] K. Svanberg, The method of moving asymptotes - a new method for structural optimization, Internat. J. Numer. Methods Engrg. 24 (1987) 359–373.
[59] P. Croaker, A. Skvortsov, N. Kessissoglou, A simple approach to estimate flow-induced noise from steady state CFD data, in: Proceedings of Acoustics, 2011, pp. 1–8.